②

AD-A225 409

NAVAL POSTGRADUATE SCHOOL
Monterey, California

THESIS

EXPERIMENTAL STUDIES OF CIRCULAR
VISCOELASTIC WAVEGUIDE ABSORBERS
FOR PASSIVE STRUCTURAL DAMPING

by

Stephen J. Watson

December 1989

Thesis Advisor: Y.S. Shin

---

90 08 1 1

Unclassified

SECURITY CLASSIFICATION OF THIS PAGE

REPORT DOCUMENTATION PAGE	Form Approved OMB No 0704-0188

1a REPORT SECURITY CLASSIFICATION UNCLASSIFIED	1b RESTRICTIVE MARKINGS

2a SECURITY CLASSIFICATION AUTHORITY	3 DISTRIBUTION/AVAILABILITY OF REPORT Approved for Public Release; Distribution is Unlimited
2b DECLASSIFICATION/DOWNGRADING SCHEDULE	

4 PERFORMING ORGANIZATION REPORT NUMBER(S)	5 MONITORING ORGANIZATION REPORT NUMBER(S)

6a NAME OF PERFORMING ORGANIZATION Naval Postgraduate School	6b OFFICE SYMBOL (If applicable) 62	7a NAME OF MONITORING ORGANIZATION Naval Postgraduate School

6c ADDRESS (City, State, and ZIP Code) Monterey, CA 93943-5000	7b ADDRESS (City, State, and ZIP Code) Monterey, CA 93943-5000

8a NAME OF FUNDING/SPONSORING ORGANIZATION	8b OFFICE SYMBOL (If applicable)	9 PROCUREMENT INSTRUMENT IDENTIFICATION NUMBER

8c ADDRESS (City, State, and ZIP Code)	10 SOURCE OF FUNDING NUMBERS			
	PROGRAM ELEMENT NO	PROJECT NO	TASK NO	WORK UNIT ACCESSION NO

11 TITLE (Include Security Classification)
Experimental Studies of Circular Viscoelastic Waveguide Absorbers for Passive Structural Damping

12 PERSONAL AUTHOR(S)
Watson, Stephen James

13a TYPE OF REPORT Master's Thesis	13b TIME COVERED FROM ___ TO ___	14 DATE OF REPORT (Year, Month, Day) December 1989	15 PAGE COUNT 72

16 SUPPLEMENTARY NOTATION The views expressed in this thesis are those of the author and do not reflect the official policy or position of the Department of Defense or the U.S. Government.

17 COSATI CODES			18 SUBJECT TERMS (Continue on reverse if necessary and identify by block number)
FIELD	GROUP	SUB-GROUP	Waveguide Absorber, Viscoelastic, Damping

19 ABSTRACT (Continue on reverse if necessary and identify by block number)

The U.S.Navy continues to investigate and develop better methods for ship noise and vibration reduction. One such method is the introduction of waveguide absorbers. This research is a continuation with the use of viscoelastic waveguide absorbers as a means of reducing the vibrational energy developed within a plate like structure, such as a ship's hull between frames and longitudinals.

The effects of temperature and size of circular viscoelastic

20 DISTRIBUTION/AVAILABILITY OF ABSTRACT ☒ UNCLASSIFIED/UNLIMITED ☐ SAME AS RPT ☐ DTIC USERS	21 ABSTRACT SECURITY CLASSIFICATION Unclassified
22a NAME OF RESPONSIBLE INDIVIDUAL Y. S. Shin	22b TELEPHONE (Include Area Code) (408) 373-2341	22c OFFICE SYMBOL 69Sg

DD Form 1473, JUN 86   Previous editions are obsolete   SECURITY CLASSIFICATION OF THIS PAGE

S/N 0102-LF-014-6603

Unclassified

Block 19 cont.

waveguide absorbers, on the driving point impedance were
studied and the test results were compared with a previously
developed computer prediction model with very favorable
agreement. A study for the development of the scheme for
the selection of waveguide absorbers and for the decision of
the attachment locations for the maximum vibration reduction
based on the waveguide absorber loss factor equation was also
performed. One, Two, and three waveguide absorbers were
attached to a vibrating plate at chosen locations based on
impedance matching and plate velocity, to confirm the use
of the loss factor equation. Experimental results showed
significant reduction of vibration at resonant frequencies.

EXPERIMENTAL STUDIES OF CIRCULAR VISCOELASTIC WAVEGUIDE ABSORBERS FOR PASSIVE STRUCTURAL DAMPING

by

Stephen James Watson
Lieutenant , United States Navy
B.S.M.E., United States Naval Academy, 1982

Submitted in partial fulfillment of the
requirements for the degree of

MASTER OF SCIENCE IN MECHANICAL ENGINEERING

from the

NAVAL POSTGRADUATE SCHOOL
December 1989

Author: _____
Stephen James Watson
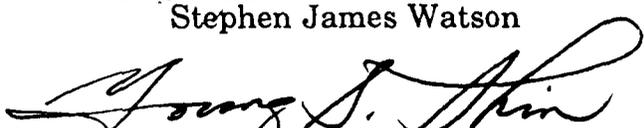
Approved by: _____
Y.S. Shin, Thesis Advisor
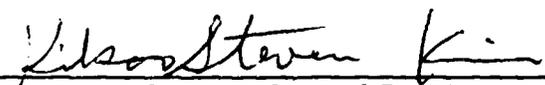
_____
K.S. Kim, Second Reader
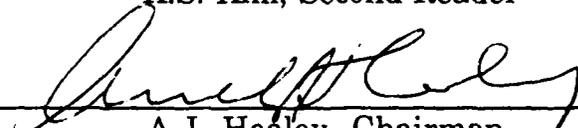
_____
A.J. Healey, Chairman,
Department of Mechanical Engineering

Accession For	
NTIS GRA&I	☑
DTIC TAB	☐
Unannounced	☐
Justification	
By	
Distribution/	
Availability Codes	
Dist	Avail and/or Special
A-1	

iii

ABSTRACT

The U.S.Navy continues to investigate and develop better methods for ship noise and vibration reduction. One such method is the introduction of waveguide absorbers. This research is a continuation with the use of viscoelastic waveguide absorbers as a means of reducing the vibrational energy developed within a plate like structure, such as a ship's hull between frames and longitudinals.

The effects of temperature and size of circular viscoelastic waveguide absorbers, on the driving point impedance were studied and the test results were compared with a previously developed computer prediction model with very favorable agreement. A study for the development of the scheme for the selection of waveguide absorbers and for the decision of the attachment locations for the maximum vibration reduction based on the waveguide absorber loss factor equation was also performed. One, two, and three waveguide absorbers were attached to a vibrating plate at chosen locations based on impedance matching and plate velocity, to confirm the use of the loss factor equation. Experimental results showed significant reduction of vibration at resonant frequencies.

TABLE OF CONTENTS

ACKNOWLEDGEMENTS

I. INTRODUCTION

A.   BACKGROUND

The long standing desire of the Navy to reduce noise and vibrations, particularly low frequency vibrations transmitted into the water, has generated some interesting and diverse methods and approaches.

This research is a continuation in the area of vibration reduction through the use of viscoelastic waveguide absorbers mounted on a vibrating structure at selected points with a small stud mount to transfer energy from the structure to the damping material. The viscoelastic material absorbs structural vibration energy through the point of attachment and dissipates this energy in the form of heat caused by shear stress. The novelty of this approach to damping is the simplicity of application and the effectiveness in the broadband frequency range with relatively less material. Each absorber can be attached quickly and easily at one or more points on the structure, while it is impossible for some of the current methods of securing the damping material over large surface areas.

B.   PREVIOUS WORK

Research had been conducted in this area of vibration damping prior to 1983. However, the main thrust in this particular direction was reported by Ungar and Kurzweil [Ref. 1] in which they introduced the use of a tapered beam of thin aluminum laminated with viscoelastic material as shown in Figure 1. They worked with a tapered beam because they expected that design to be lighter in weight and to display more effective damping than a uniform cross-sectioned beam. Their results were

favorable but somewhat inconclusive since they did not take into account the viscoelastic properties of the damping material and, as a result, their theoretical prediction for driving point impedances varied widely from experimental results.
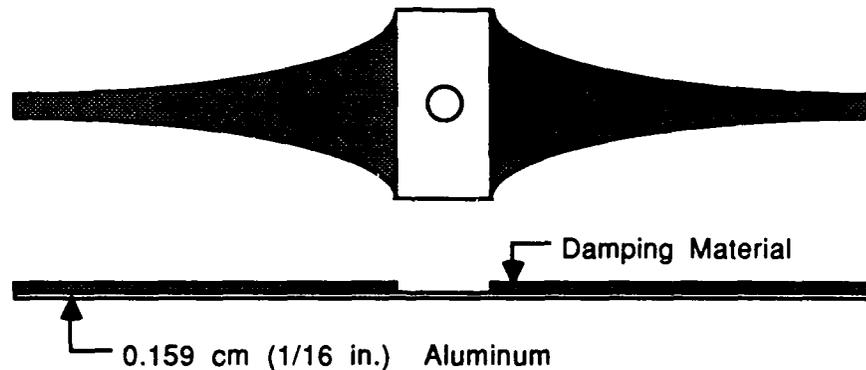
Figure 1. Tapered Beam with Damping Material.

Lee [Ref. 2] conducted initial experimentation at the Naval Postgraduate School in early 1988 with two types of beam waveguide absorbers; a viscoelastic beam and a constrained layer beam. He concluded that the beam will reduce vibrations in a test plate over a wide frequency range (100Hz-2000Hz) and that the reduction is additive based on the number of beams attached to the plate. Figure 2 shows the basic construction of the two types of beams used.
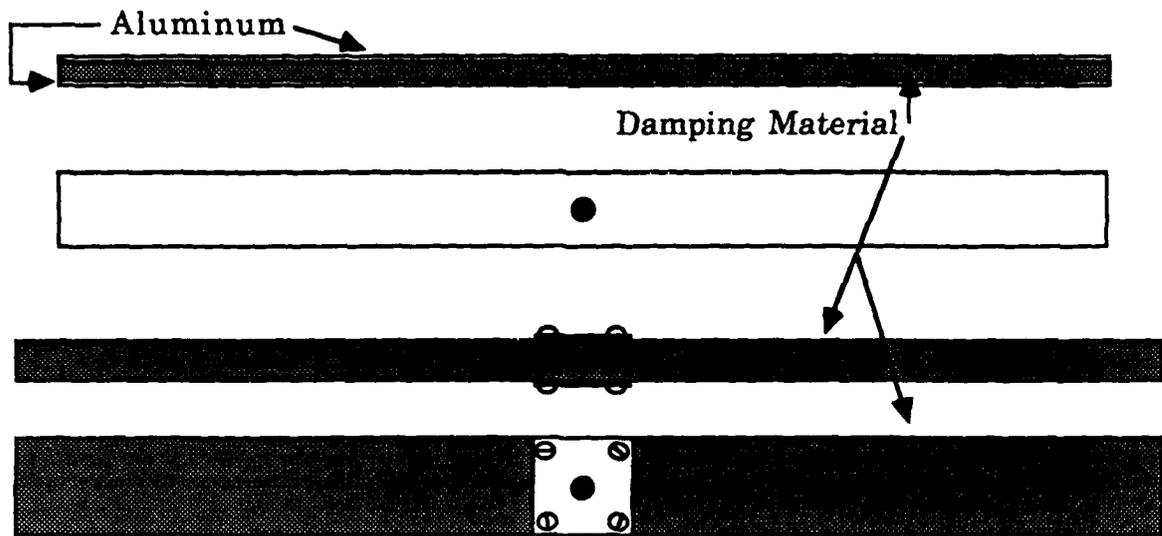
Figure 2. Constrained Layer and Single Layer Beams.

Horne [Ref.3] conducted similar research as Lee with beam waveguide absorbers while also conducting a modal survey on the test structure which was a thin aluminum rectangular plate with fixed boundary conditions. The approach was to determine the mode shapes of the test plate in order to determine ideal locations for the waveguide dampers. Figure 3 shows a relative perspective of the deflections in the plate as viewed from the edge if the plate were sliced lengthwise at section 6. Horne concluded that by attaching a damper to a plate anti-node point, the modal damping was increased. Furthermore,the magnitude of the increased damping was dependent upon the number and type of dampers attached to anti-node points and their orientation.

3
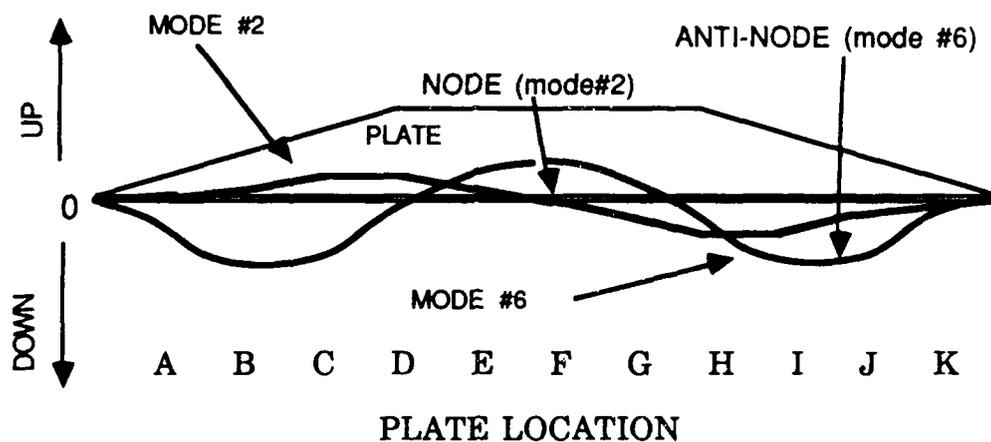
Figure 3. Exaggerated Relative Deflections across Section 6 of the Plate (not to scale).

Hettema [Ref.4] conducted research on a circular waveguide absorber. He developed a theory on a circular viscoelastic waveguide absorber and a computer program which would predict the driving point impedance of a disk given the material characteristics, geometry, and temperature. Armed with this computer prediction tool, Hettema was able to conclude that the impedance of a disk is greatly effected by the temperature of the disk. However, he did not verify experimentally the actual effect of temperature variations.

C.   CURRENT WORK

In this study the impedances of the circular viscoelastic waveguide absorbers were evaluated experimentally at different temperatures to verify Hettema's computer predictions. The application of the waveguide absorbers in the most effective manner to maximize damping of the structure is also studied in this work. This procedure incorporates a combination of anti-node placement and impedance matching to maximize

damping. Throughout this thesis the disks used will be refered to by a pair of numbers. The first number refers to the disk radius and the second number refers to the disk thickness. An example would be a reference for a 12.7 x 0.635 cm (5 x 0.25 in.) disk which indicates a 12.7 cm (5 in) radius and 0.635 cm (0.25 in) thickness. Figure 4 illustrates the identification code used for the disks. Table 1.1 lists all the disks used in this study in both SI and English units for easy comparison. The 15.2 cm (6 in) radius was the maximum radius possible due to the damping material size availability from the manufacturer.

RADIUS = 15.2 cm
(6 in)

THICKNESS = 0.953 cm = 3/8" = 0.375"
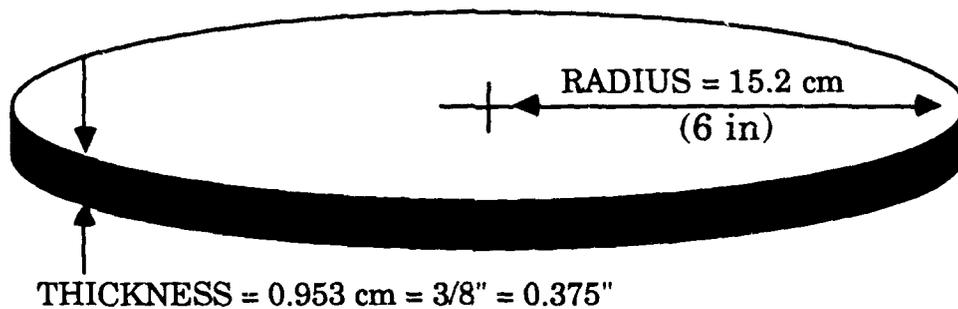
DISK SIZE = (RADIUS) x (THICKNESS)
= 15.2 x 0.953 cm (6 x 0.375 inch)

Figure 4. Disk Identification Method.

Units: Inches	centimeters
6 x 0.375	15.2 x 0.953
5 x 0.375	12.7 x 0.953
4 x 0.375	10.2 x 0.953
6 x 0.25	15.2 x 0.635
5 x 0.25	12.7 x 0.635
4 x 0.25	10.2 x 0.635

Table 1.1 Comparison of Units.

II. THEORY

A. LOSS FACTOR

Ungar and Kurzweil [Ref. 1] developed equation 2.1 to determine the damping loss factor contribution of a waveguide absorber, η to a structure which is a function of V_S, the velocity of the structure at the attachment point, V_M, the mass-distribution-weighted spatially averaged structural velocity amplitude, M_S, the total mass of the structure, ω, the frequency, Z_S, the complex impedance of the structure at the attachment point, Z_A, the complex impedance of the absorber system, and R_A, the real part of the impedance of the absorber, where $Z_A = R_A + j\,I_A = F/V$, and $j = \sqrt{-1}$.

$$\eta = \frac{R_A}{\omega M_s} \frac{\left|\dfrac{V_S}{V_M}\right|^2}{\left|1 + \dfrac{Z_A}{Z_S}\right|^2} \tag{2.1}$$

The four major factors considered (in order to maximize frequency response reduction) in this equation are V_S, the structure velocity, R_A, the real part of the absorber impedance, Z_A, the absorber impedance, and Z_S, the structure impedance, while the fifth factor M_S can be considered constant for each case and each selected point on the structure. The final factor V_M would have been a somewhat difficult variable to calculate since the dynamic mass of the damping disk, acting through the driving point impedance, changed with the changing temperature. However, for initial rough estimates, in order to reduce resonant frequency magnitudes, the factors V_S and Z_A/Z_S were focused on. The basic approach to maximize the structure damping was based on the combined effect of the first four factors

7

listed previously. To achieve the maximum loss, the structure velocity must be a maximum (an anti-node location), the real driving point impedance of the damper must be a maximum, and the complex impedance ratio Z_A/Z_S must be as small as possible.

B.   TEST PLATE ANTI-NODE LOCATION

Equation 2.1 clearly shows that the loss factor for the structure will become zero when the waveguide is attached to a node point since the structural velocity V_S at a node point is zero. Conversely, the loss factor should have a greater probability of being a maximum value when the waveguide is attached to an anti-node due to the maximum structural velocity occurring at anti-nodes.

Modes for the structure were previously determined experimentally by Horne [Ref. 3] and that information is used in this study to determine the best locations for the waveguide absorbers.

C.   DISK AND PLATE IMPEDANCE MATCHING

The first approach to the complex impedance ratio Z_A/Z_S was to make this ratio as small as possible which would reduce the denominator in equation 2.1 and thus increase the damping loss factor η. However, in order to accomplish this reduction the impedance of the absorber must be small compared to the impedance of the structure at the point of attachment, and this will have the undesired effect of reducing the real impedance of the absorber R_A and cause the loss factor to decrease. Conversely, an attempt to increase the real impedance of the absorber results in an increase in Z_A raising the impedance ratio which has a greater negative effect upon the loss factor since this term is squared in the

8

denominator. Therefore, there was a greater possibility of maximum transfer of energy when the driving point impedances were closely matched. This has been the primary focus of the experimentation in this report.

D.   DISK IMPEDANCE PREDICTION

The method used to predict the impedance of the dampers was a computer programed by Hettema [Ref. 4]. This program requires the input of the dimensions and the temperature of the circular viscoelastic waveguide absorber and produces the magnitude driving point impedance data, the real driving point impedance data, the imaginary data, and the db data for the frequency limits specified. Figure 5 is a reproduction of the computer program flow chart from reference 4. Additional data for the viscoelastic material normally required to solve for this type of information was stored within the program. Therefore, a different damping material other than the material used in this study, would require some simple modifications to the data in the program.
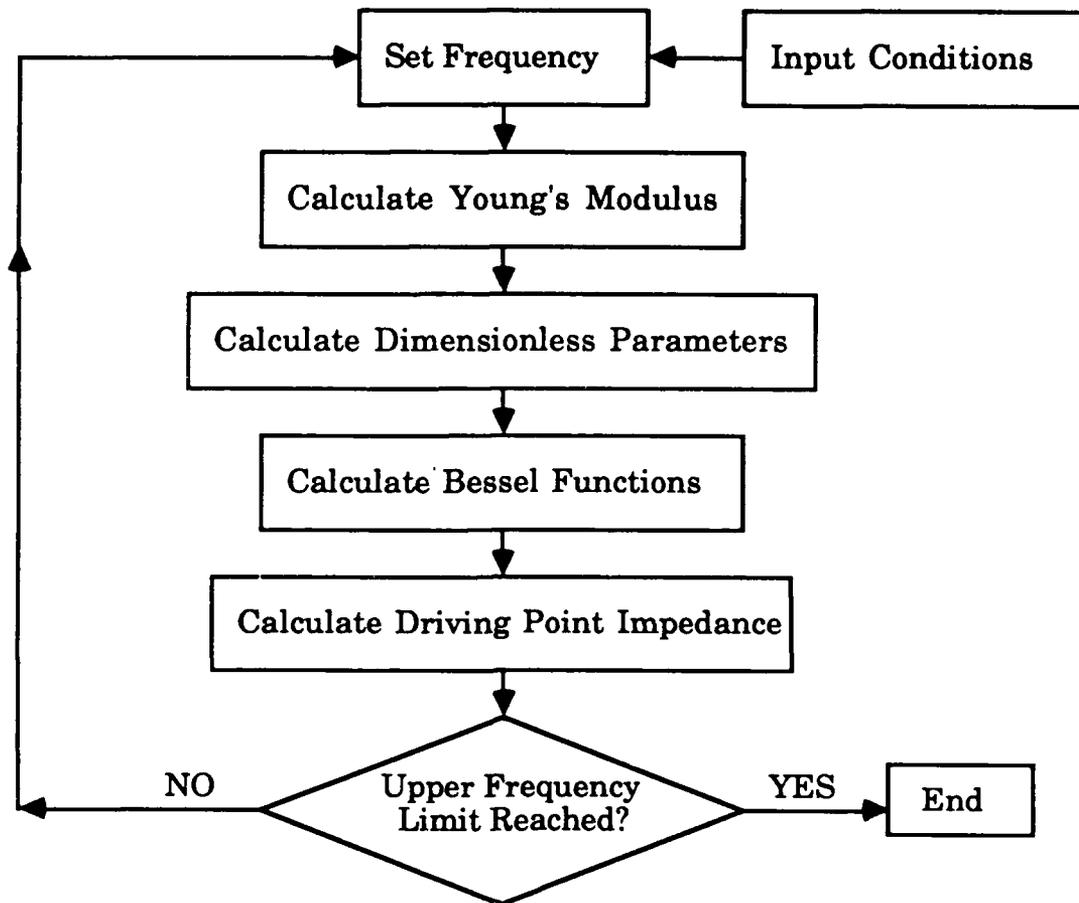
Figure 5. Flow Chart for FORTRAN Program.

III. EXPERIMENTAL METHOD

A. TEMPERATURE CONTROL CHAMBER

A temperature control chamber (fig. 6) was designed and constructed to maintain a constant ambient temperature for the viscoelastic damping material while allowing vibration tests within this environment. The chamber was adapted from a box originally constructed from 1.3 cm (0.5 inch) plywood with 2.5 x 10 cm (approximately 1x4 inch) wood outside bracing for structural strength. A removable front panel was created for access. A twin fan, double coil heat exchanger was mounted in the upper left corner of the chamber, as shown in Figure 6, to allow the transfer of energy between the air inside the chamber and the fluid in the heat exchanger coils. This arrangement created a slow but steady temperature control for the environment within the chamber once the front panel had been secured in place. A refrigeration circulation bath was connected to the heat exchanger through two short 1.27 cm (0.5 inch) ID flexible hoses. An approximately 50% water - 50% ethylene glycol liquid mixture was used as the transfer medium through the bath and coils. The ethylene glycol was introduced as a safety measure to protect the recirculation bath pump when operating the chamber at temperatures below 10° C (50° F). Extensive testing over 3 days with thermocouples verified the ability of the chamber to maintain a constant inner ambient temperature within +/- 0.6° C (1° F) indefinitely for temperatures between 4° C (40° F) and 37° C (99° F).
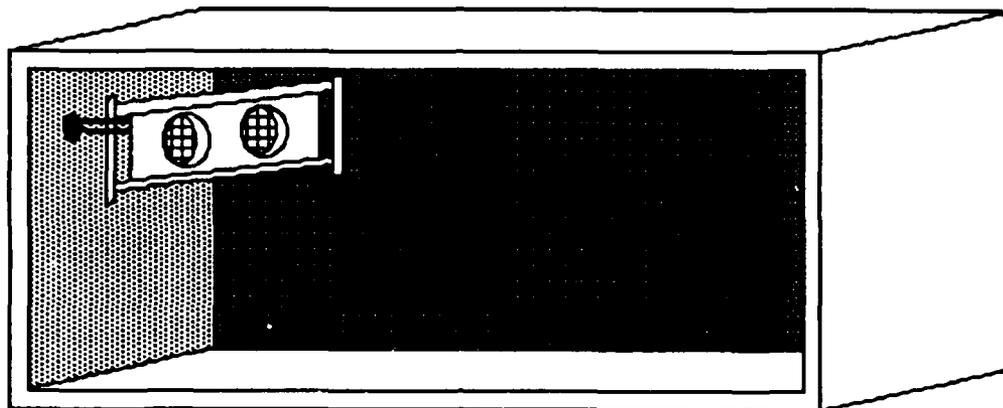
Figure 6. Temperature Control Chamber (front panel removed).

B. EXPERIMENTAL SET UP

### 1. Viscoelastic Waveguide Absorbing Disks

A total of 6 viscoelastic disks were tested as waveguide absorbers in this study. Two different thicknesses of material were used, 0.636 cm (0.25 in.) and 0.953 cm (0.375 in.) coupled with three different radii, 10.2 cm, 12.7 cm, and 15.2 cm (4 ,5, and 6 in.). The disks were all the same material obtained from the United McGill Corporation [Ref. 6] as Soundscreen Noise Damping tile. The material was cut to form a circular disk with uniform thickness for each of the six cases. The initial steps in this study were to determine the driving point impedances for the waveguide disks. This was accomplished using a Wilcoxon Research (WR) vibration generator, model F7/F4 mounted in a test stand. The disks were attached with the waveguide mount to the head of the vibration generator (fig. 7) which was then placed inside the controlled temperature chamber. The four cables leading from the generator were passed through a small access port in the side of the chamber. The F7 and F4 cables were attached to the WR N7/N9 matching network which was connected to the WR PA7 power amplifier.
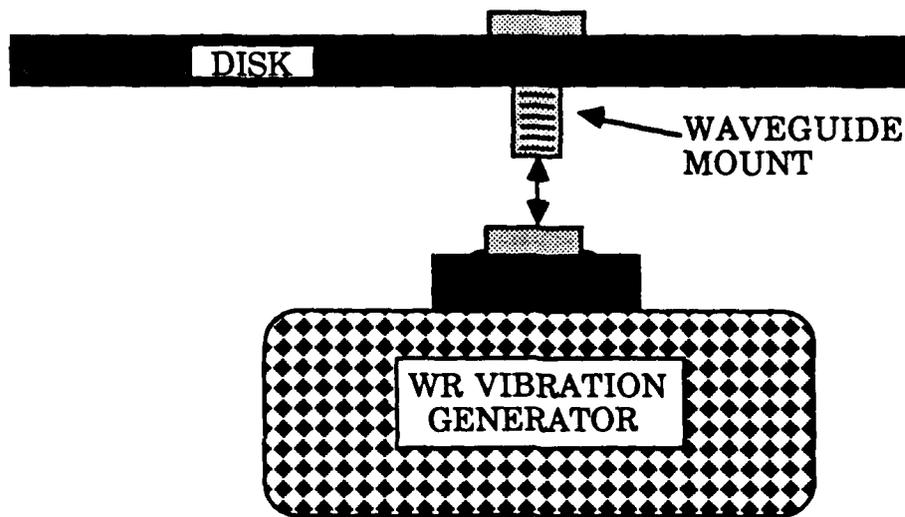
Figure 7. Waveguide Damper Mounted to Shaker.

The force transducer and accelerometer cables were each attached to a PCB Piezotronics, Inc. 462A charge amplifier. Based on the calibration data for the shaker head serial number 9514, the force charge amplifier was set for 0.219 pC/unit transducer sensitivity and 10,000 unit/V range giving an output of 44.5 N/V (10 Lbf/V). Additionally, the accelerometer charge amplifier was set for 0.5 pC/unit and 50 unit/V resulting in an output of 5 g/V.

The PA7 power amplifier was connected to a Hewlett Packard (HP) 3562A Digital Signal Analyzer (DSA) through the Source port with a coaxial cable. The force charge amplifier and the accelerometer charge amplifier were also connected to the HP 3562A DSA through Channel 1 and Channel 2 respectively. Figure 8 shows a block diagram of the set up as described.

Temperature Controlled Chamber

Disk

Force Transducer
Accelerometer

Vibration Generator
F7/F4

PCB
462A
Charge
Amp

PCB
462A
Charge
Amp

WR N7/N9
Matching
Network

PA7 Power Amplifier

Source | CH 1 | CH 2

HP 3562A Digital Signal Analyzer
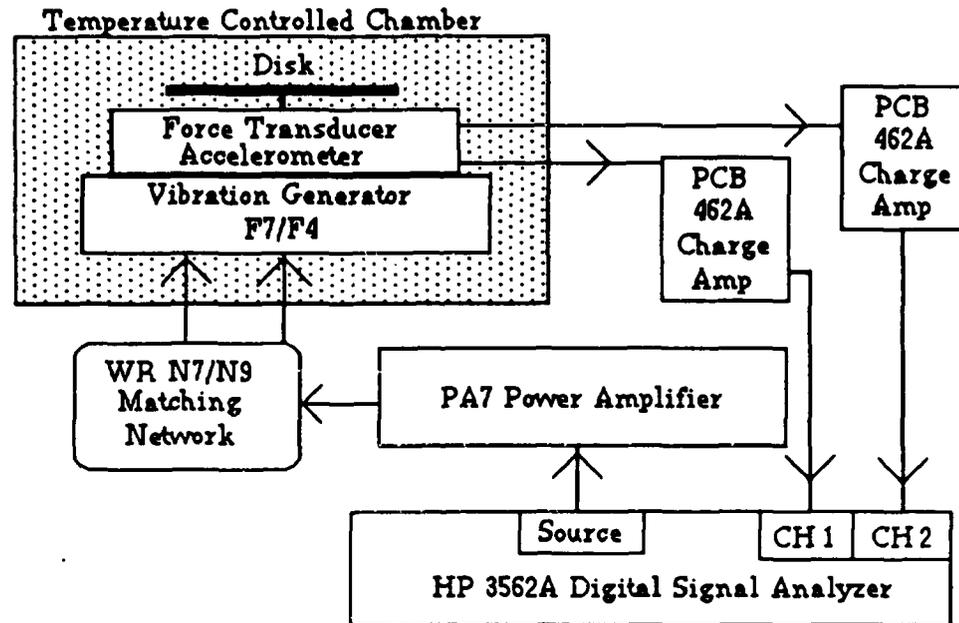
Figure 8. Experimental Set Up.

The DSA was operated in the Swept Sine mode (linear sweep) with the following functions enabled:

a)   Frequency setting 0-2000 hz with Auto resolution

b)   Source level set to 600 mV sweeping up

c)   Averages set at 10 with Auto integration

d)   Range for both channels on Auto range up

e)   Input couple for both channels set on AC

f)   Engineering units set to 100 mV/EU for channel 1 and 200 mV/EU for channel 2.

This set up was used for all 6 disks at various temperatures.

2. Test Plate Structure

The test structure used throughout this, and previous research at the Naval Postgraduate School was a 76.2 x 55.9 x 5.1 cm (30 x 22 x 2 inch)

thick aluminum slab with the area below the grid machined out from the bottom to a thickness of .794 cm (0.3125 inch) simulating a flat plate with fixed boundary conditions. The dimensions of the grid, as shown in Figure 9, were 61 x 40.6 x 0.794 cm (24 x 16 x 0.3125 inch).
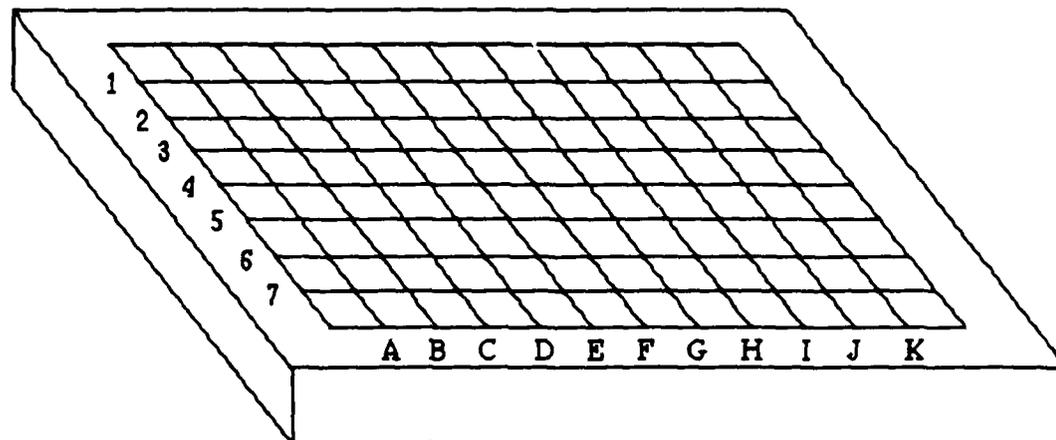
Figure 9. Aluminum Test Structure. The area under the grid was machined out to form a 0.794 cm (0.3125 in) plate.

The impedance of the plate at various points was obtained with the use of a PCB model GK291B80 impulse hammer and a PCB 302A accelerometer. The accelerometer was attached to the underside of the plate at the point of interest with petro wax to allow a clear target impact point on the top of the plate for the hammer. This method was safer for the accelerometer and slightly more accurate since the force transducer and the accelerometer were operating on a similar axis tangent to the plate. The hammer and accelerometer were both connected to a PCB model 482A05 I.C.P. power supply and subsequently to channel 1 and 2 respectively, on the DSA. Figure 10 shows the set up for testing the plate impedance.
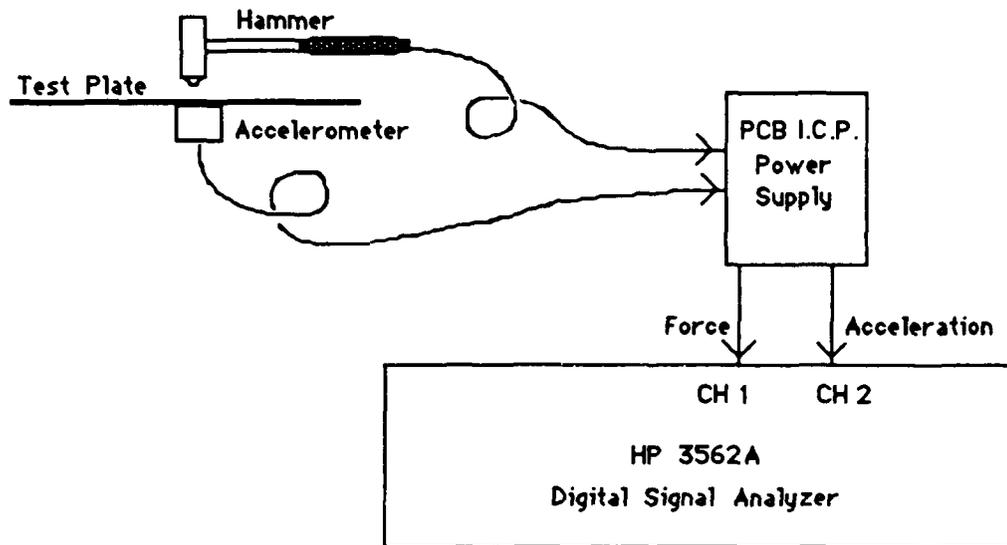
Figure 10. Plate Set Up for Impedance.

The DSA set up was for a linear response with a uniform window. 50 averages were used with the hammer acting as the triggering device for the DSA.

C.   EXPERIMENTAL TEST PLAN

The overall approach was to thoroughly test the six different disks for driving point impedance, to conduct impulse hammer tests on the aluminum plate at selected points to determine the driving point impedance, and finally to determine experimentally the reduction in frequency response resonant peaks due after attaching one or more disks to the plate at selected points.

1. Determining the Impedance of the Disks

The initial goal was to validate the driving point impedance prediction program developed by Hettema [Ref. 4]. This was accomplished

by comparing the experimentally determined driving point impedance for the different disks at 22°, 28°, and occasionally 33° Celsius (72°, 82°, and occasionally 92° F) with the computer prediction. The program uses a linear interpolation for the material behavior characteristics between 20° and 30° Celsius (68° and 86° F) and between 30° and 40° Celsius (86° and 104° F). Unfortunately, material characteristics were not available from the United McGill Corporation for any temperatures below 20° C (68° F). Ideally, material characteristics for temperatures as low as 5° C (41° F) are necessary for a complete comparison of the program capabilities.

Data was obtained on all of the disks for temperatures ranging from 6° up to 28° C (42° to 82° F) and occasionally to 33° C (92° F) and for frequencies from 0 to 2k Hz as shown in Appendix A and B. This particular temperature range was chosen as representative of the typical range of environments in which the U.S.Navy operates.

The disks were tested inside the controlled temperature chamber which was allowed to stabilize at a desired temperature and then approximately one hour of additional time was allowed to elapse prior to beginning the experimental run on the disk. This time lapse was essential to ensure that the disk material was at the same temperature as its environment prior to conducting tests. All test data was recorded on 90 mm (3.5") diskettes for later analysis.

The Frequency Response data obtained from a test run was converted to impedance through the use of the DSA Math functions. Since the frequency response, or transfer function, H(f), for these experiments was the acceleration divided by the force

$$H(f) = \frac{A}{F} \qquad (3.1)$$

and the acceleration was related to the velocity by equation 3 2.

$$A = j\omega V \qquad (3.2)$$

The impedance was easily calculated by multiplying the transfer function with $(j\omega)^{-1}$ and inverting the results on the DSA.

$$H(f) = \frac{j\omega V}{F} \qquad (3.3)$$

$$Z = \frac{F}{V} = \frac{j\omega}{H(f)} \qquad (3.4)$$

The impedance data in the DSA was then divided by the gravity factor, g, to properly scale the impedance for use in equation (2.2). The gravity factor was negative for these tests since the shaker head was inverted which resulted in the force term being applied in the negative direction with respect to normal gravity. More information can be obtained from the DSA Operating Manual [Ref. 7].

2. Detemining the Impedance of the Plate

The simplest method to determine the impedances of the plate at selected points was to use an impulse hammer since the vibration generator required a small stud mount at each point for securing it to the plate. Therefore, in order to prevent drilling and tapping holes all over the plate which would affect the response of the plate, the impulse hammer method was adopted and used effectively. After some initial practice and patience with the hammer, various points on the test plate were impacted

for frequency response data. This data was converted to driving point impedance with equation (3.6) where MSF is a hammer mass scaling factor obtained from the impulse hammer operators manual [Ref. 8].

$$Z = \frac{MSF \times j\omega}{H(f)} \qquad (3.6)$$

The base line frequency response data for all subsequent comparisons was obtained from a small WR F3 Vibration Generator (shaker) which was mounted to the plate at 2B with a small stud (the hole was previously drilled and tapped for this purpose). The remainder of the driving point impedance tests were conducted by attaching an accelerometer to the underside of the plate using petro wax, and a hammer test was conducted on the top of the plate by striking the same point 50 times with an approximately constant force for each strike. The DSA range limits automatically prevented an excessively high force strike from being entered in the averageing data which increased the accuracy of each test. Since the hammer contained a force transducer and an accelerometer was mounted below the impact point, the frequency response from the hammer test was obtained. Impulse hammer tests were completed at plate grid locations 2I, 3I, 4F, 5J, 6C, 6E, and 6J as shown in Figure 11.
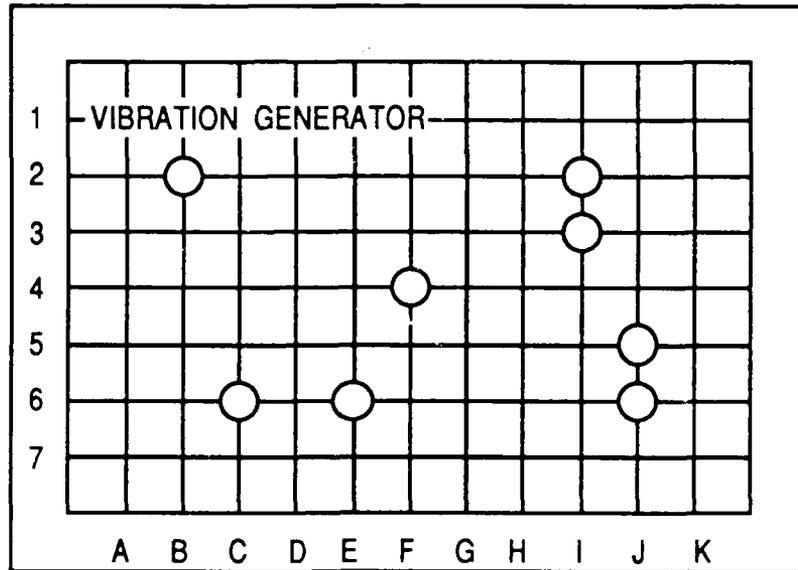
ALL FREQUENCY RESPONSE MEASUREMENTS
CONDUCTED AT POINT 2B

Figure 11. Impulse Hammer Test Points.

The driving point impedances at these locations, coupled with the disk impedance information, were used to calculate a theoretical loss factor trend which was compared with experimental results.

3. Determining the Motion of the Plate

The data for the plate motion was obtained from reference 3 which contained the results from modal analyses conducted previously on the plate. The 2nd mode of the plate is shown in Figure 12 with the selected point 6J marked for comparison.
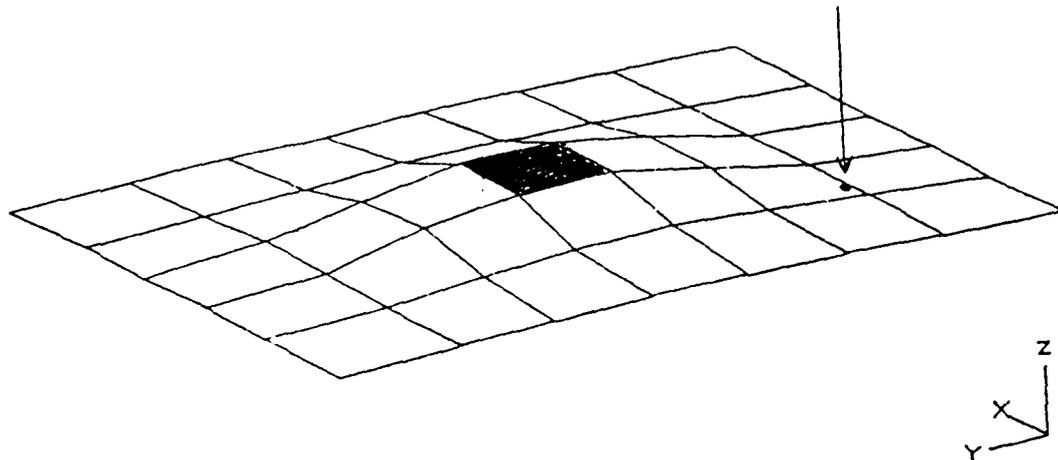
Figure 12. Plate Mode For 276.04 Hz. The shaded area represents the highest motion in the plate. The arrow indicates the location of point 6J.

The mounting point 6J was chosen based on an estimated maximum plate motion averaged between the plate frequencies of interest which included the largest magnitude resonances at 1001, 1060, 1388, and 1824 Hz (9th, 10th, 12th, and 18th modes respectively) as shown in the magnitude and phase frequency response plot of the undamped plate (fig. 13).
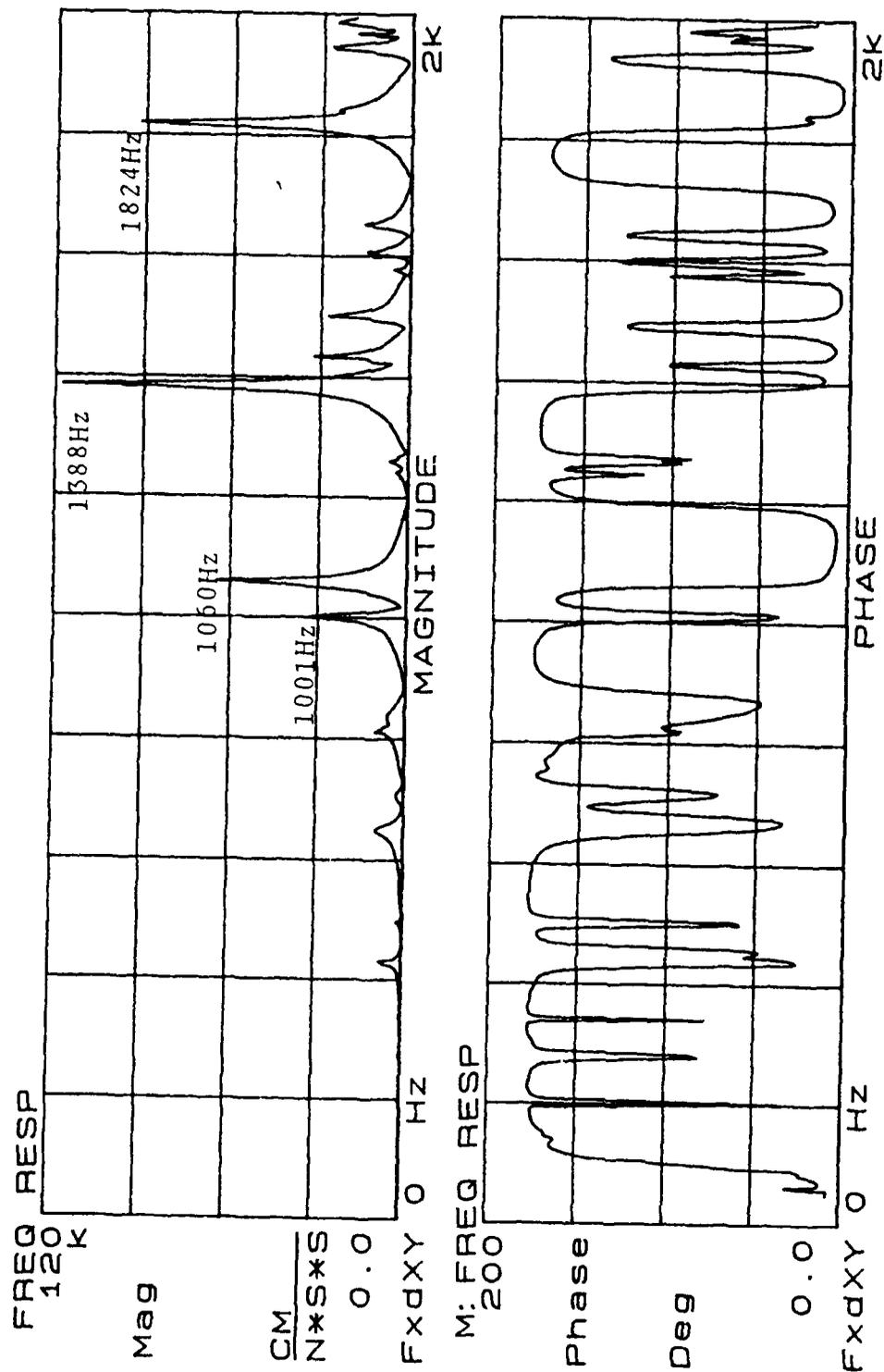
Figure 13. Undamped Frequency Responce of the Test Plate (magnitude and phase plots).

The 9th and 10th plate modes, for example, indicated a moderate plate motion at approximately 6J for 1001 and 1060 Hz respectively (figs. 14 and 15), which are both prominent peaks on the magnitude frequency response plot.
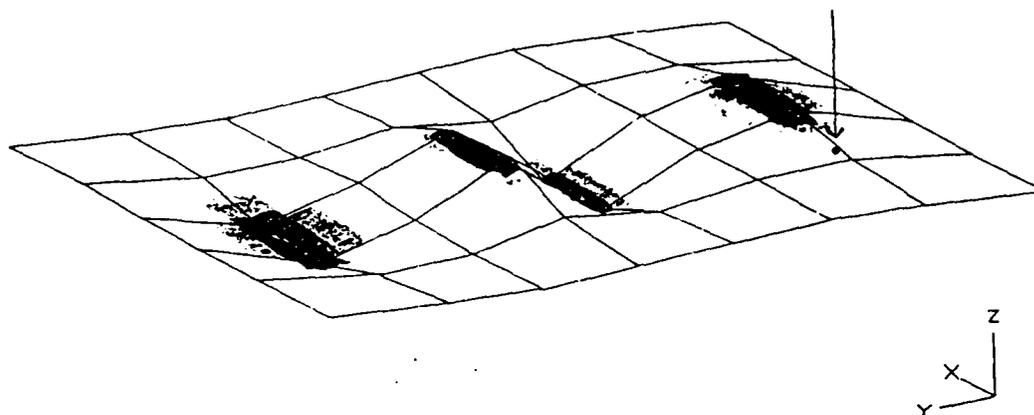
Figure 14. Plate Mode for 1001 Hz (9th Mode). The shaded area represents the highest motion in the plate. The arrow indicates the location of point 6J.
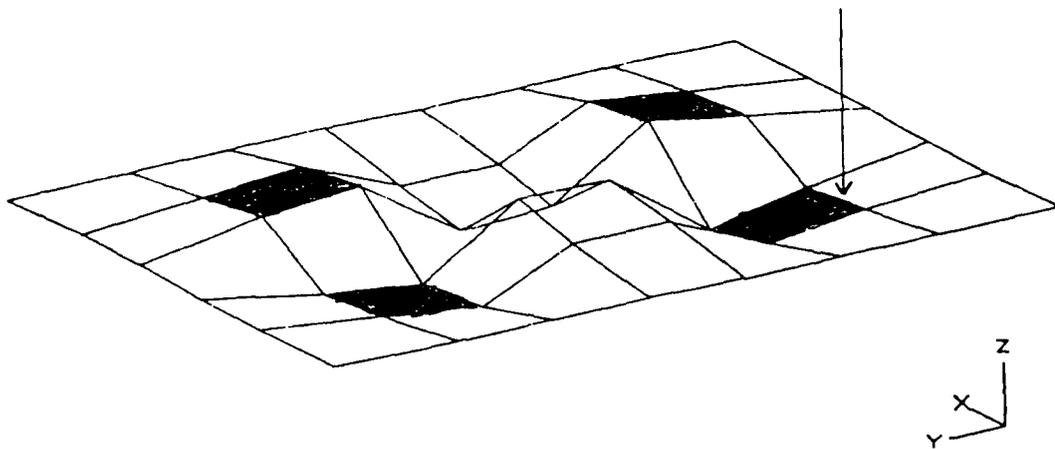
Figure 15. Plate Mode for 1060 Hz (10th Mode). The shaded area represents the highest motion in the plate. The arrow indicates the location of the point 6J.

IV. RESULTS

A. IMPEDANCE PREDICTION BY COMPUTER

Figures 16 and 17 show the experimental versus theoretical driving point impedance plots of the smallest disk (10.2 x 0.635 cm) at 22° C (72° F) and 28° C (82° F). The driving point impedance for the smallest disk compares favorably with the computer prediction at the temperatures tested. The slight difference between the experimental and theoretical driving point impedance magnitudes was possibly due to slight temperature differences between the actual test and the prediction of the computer modeling. The damping material used was extremely sensitive to temperature variations which can be seen in the experimental driving point impedance plots in appendix A. Secondly, as noted previously, the computer program uses *linear interpolation to* determine the material characteristics between the three temperatures of 20°, 30°, and 40° Celsius (68°, 86°, and 104° F). This method of linear interpolation was the only course of action available since the material characteristics were not available from the manufacturer for other temperatures. Lastly, the material characteristics from the manufacturer may have been slightly in error. Additional comparisons of the driving point impedance between the computer prediction method and the experimental method were conducted on some of the other disks as shown in figures 18 and 19 with similarly favorable results.
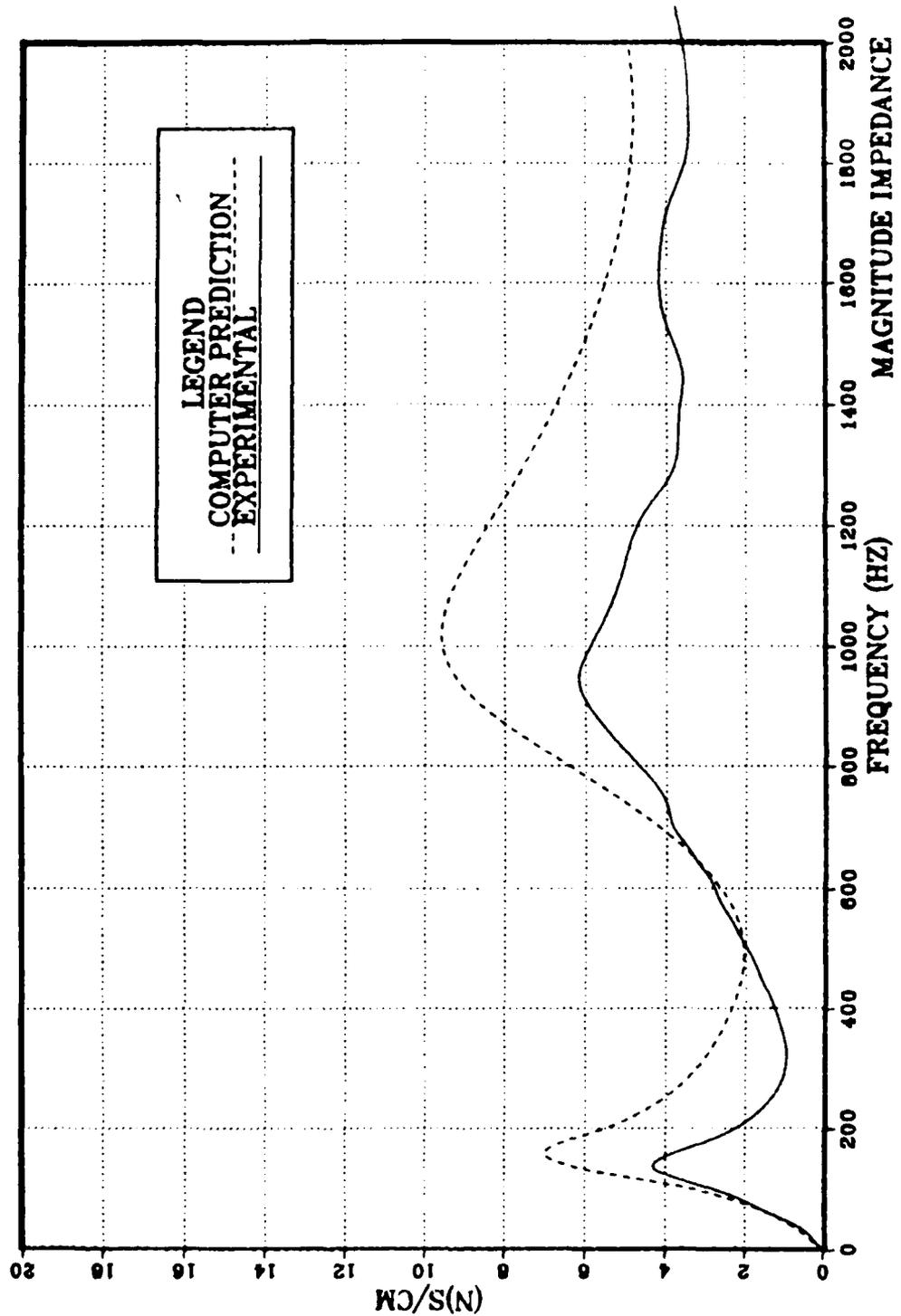
Figure 16. Driving Point Impedance for the 10.2 x 0.635 cm (4 x 0.25 in.) Disk at 22° C (72° F). Computer generated (dotted line) versus Experimental (solid line).
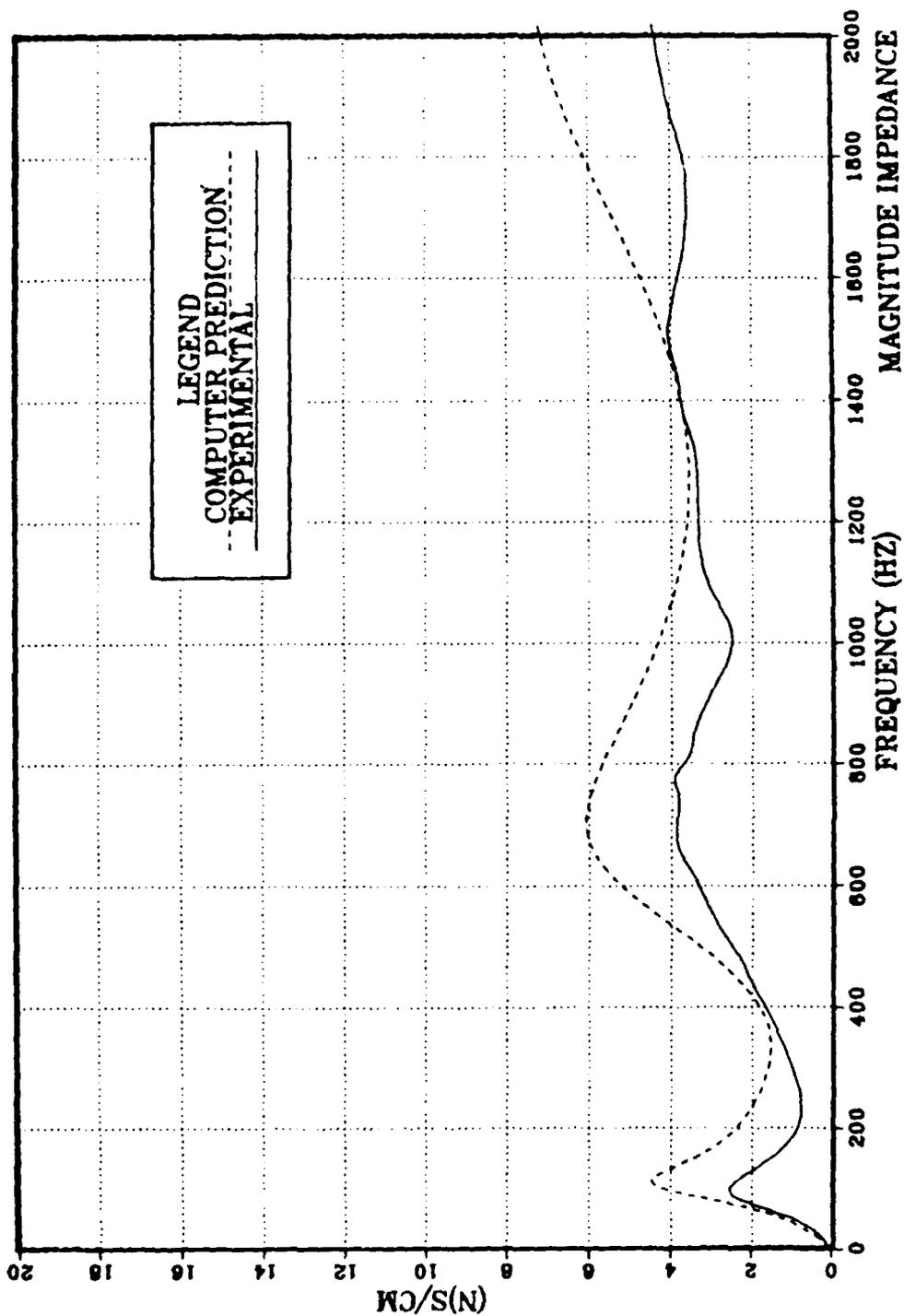
Figure 17. Driving Point Impedance for the 10.2 x 0.635 cm (4 x 0.25 in.) Disk at 28° C (82° F). Computer generated (dotted line) versus Experimental (solid line).

27
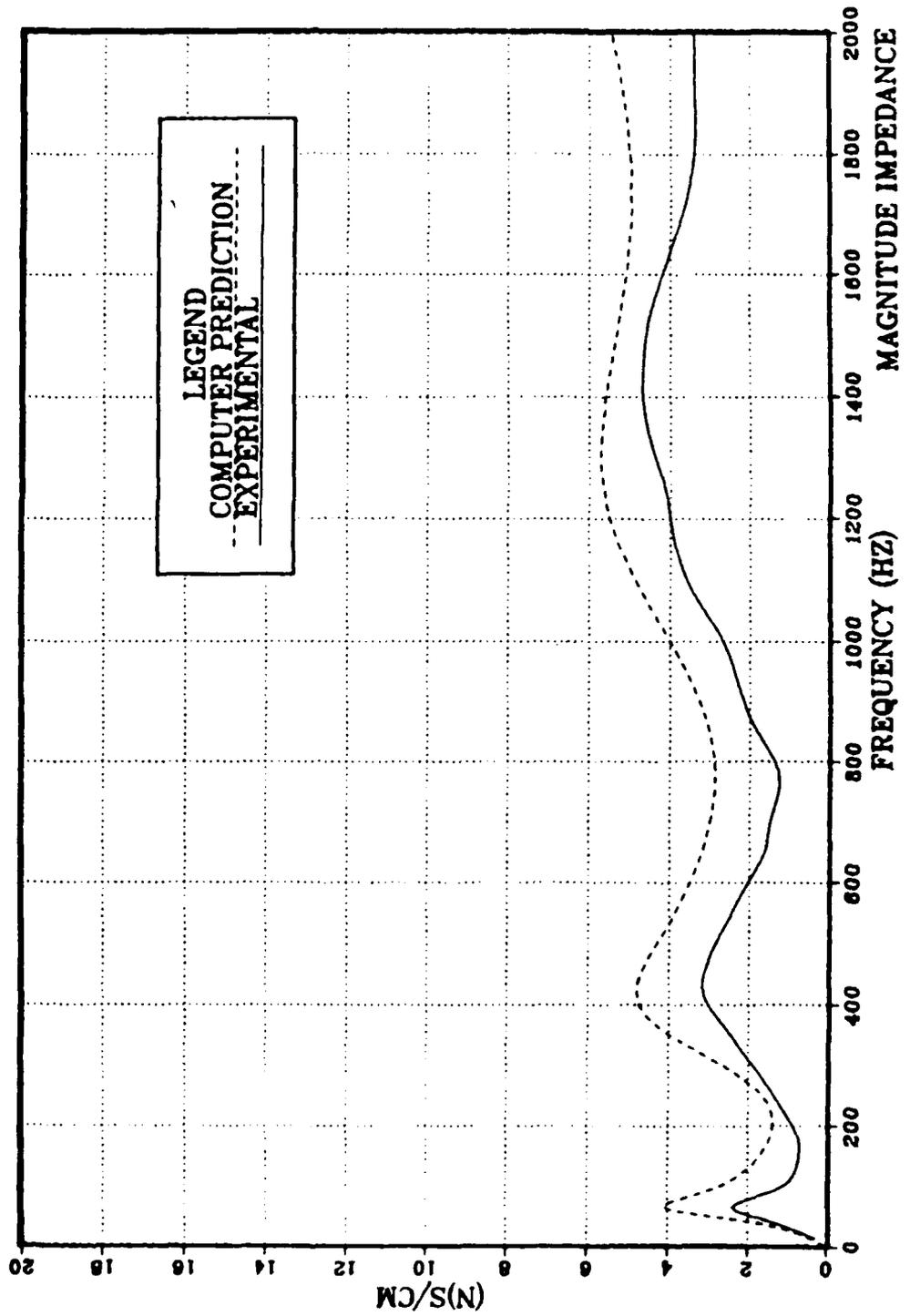
Figure 18. Driving Point Impedance for the 12.7 x 0.635 cm (5 x 0.25 in.)
Disk at 28° C (82° F). Computer generated (dotted line) versus Experimental
(solid line).
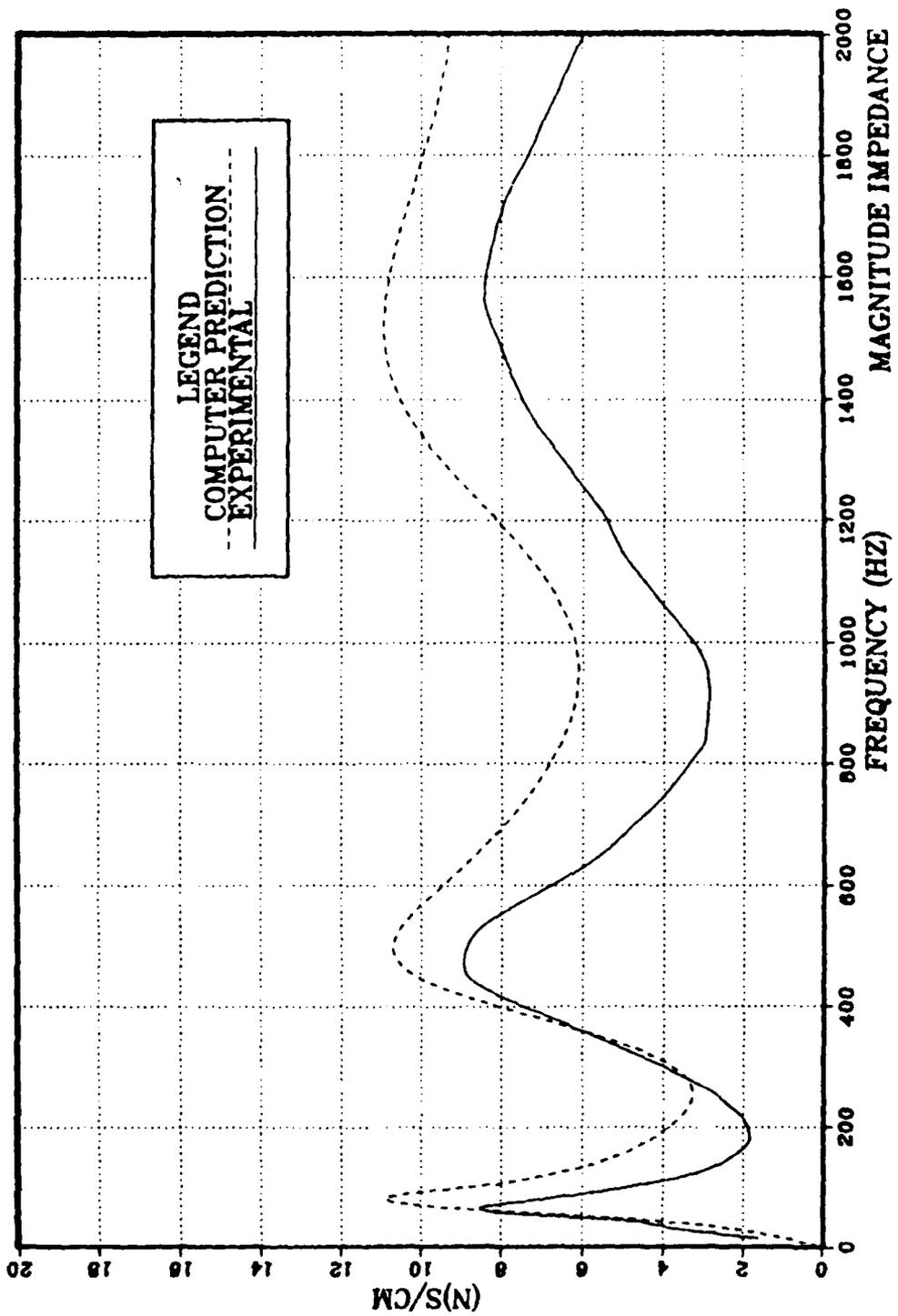
Figure 19. Driving Point Impedance for the 15.2 x 0.953 cm (6 x 0.375 in.) Disk at 24° C (75° F). Computer generated (dotted line) versus Experimental (solid line).

29

B. IMPEDANCE OF THE VISCOELASTIC WAVEGUIDE ABSORBER

The results from the experimental tests conducted on the viscoelastic waveguide absorbers at five different temperatures are contained in Appendix A. The combined impedance plots for the different absorbers indicate a reduction in the average impedance magnitude as the disk temperature increases. A characteristic rolling plot was observed for each disk regardless of size or temperature. The combined impedance plots for the 15.2 x 0.953 cm (6 x 0.375 in.) absorber for different temperatures are shown in Figure 20.
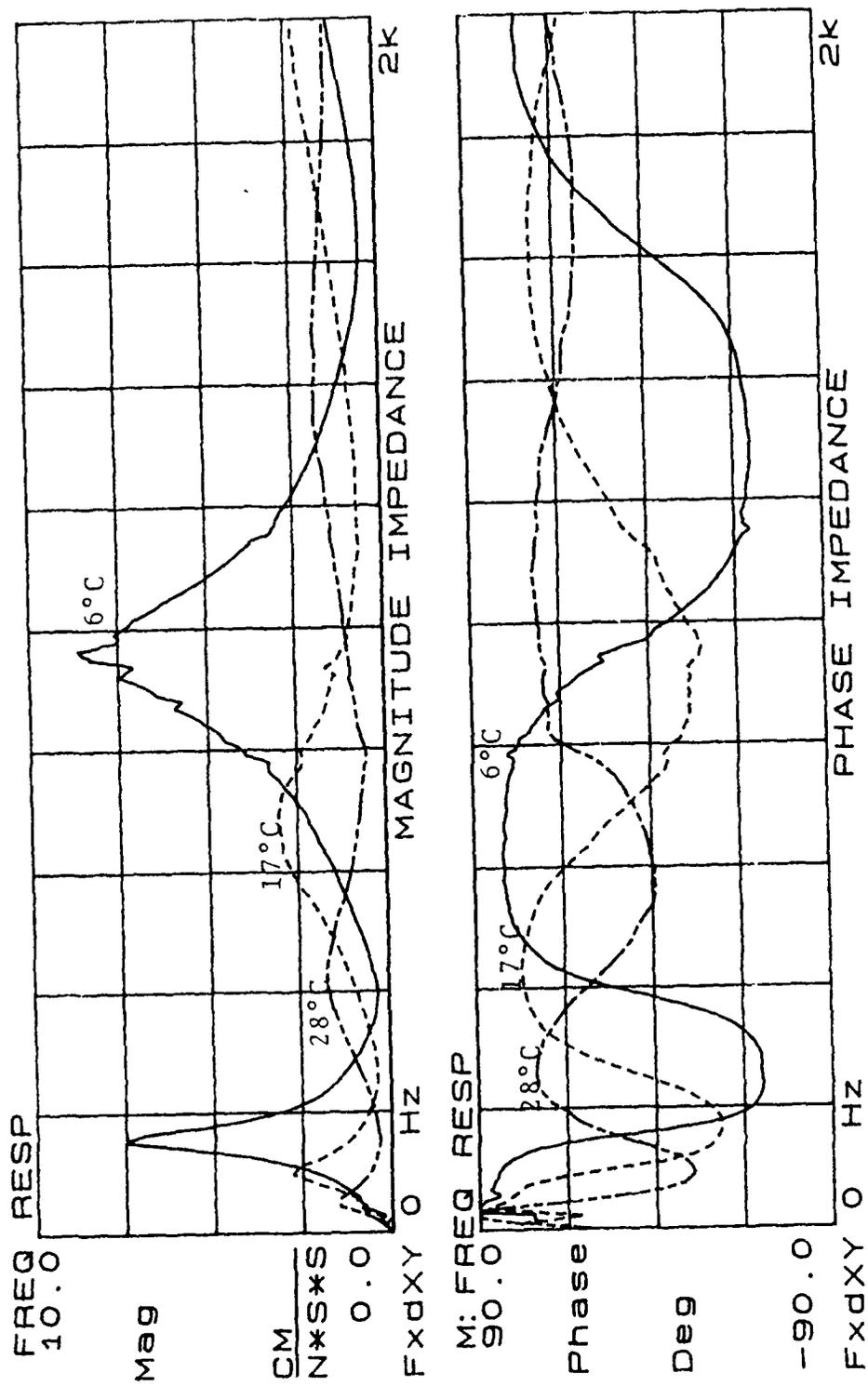
Figure 20. Combined Impedance Plots of Different Temperatures for the 15.2 x 0.953 cm (6 x 0.375 in.) Absorber.

C. FREQUENCY RESPONSE OF THE PLATE WITH WAVEGUIDE(S) ATTACHED

The introduction of the 15.2 x 0.953 cm (6 x 0.375 in.) waveguide absorber at 28° C (82° F) to the structure grid point 6J as shown in Figure 21 reduced the resonance of the 9th and 10th modes significantly.
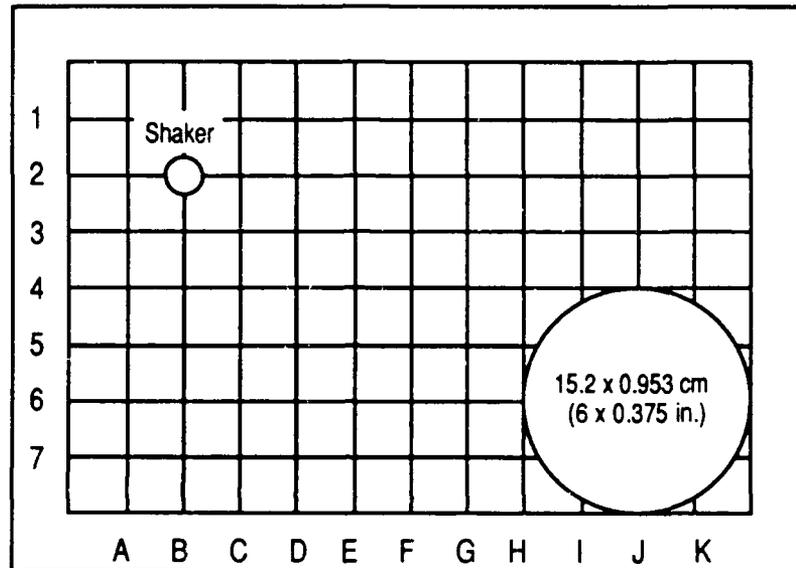
Figure 21. Waveguide Absorber mounted on Test Plate.

The attachment point 6J was chosen since it indicated moderate plate motion for the 9th and 10th modes of 1001 Hz and 1060 Hz respectively. The temperature 28° C (82° F) was chosen because the impedance of the waveguide absorber at that temperature was the closest to the impedance of the plate at location 6J for the 9th and 10th modes as shown in Figure 22.
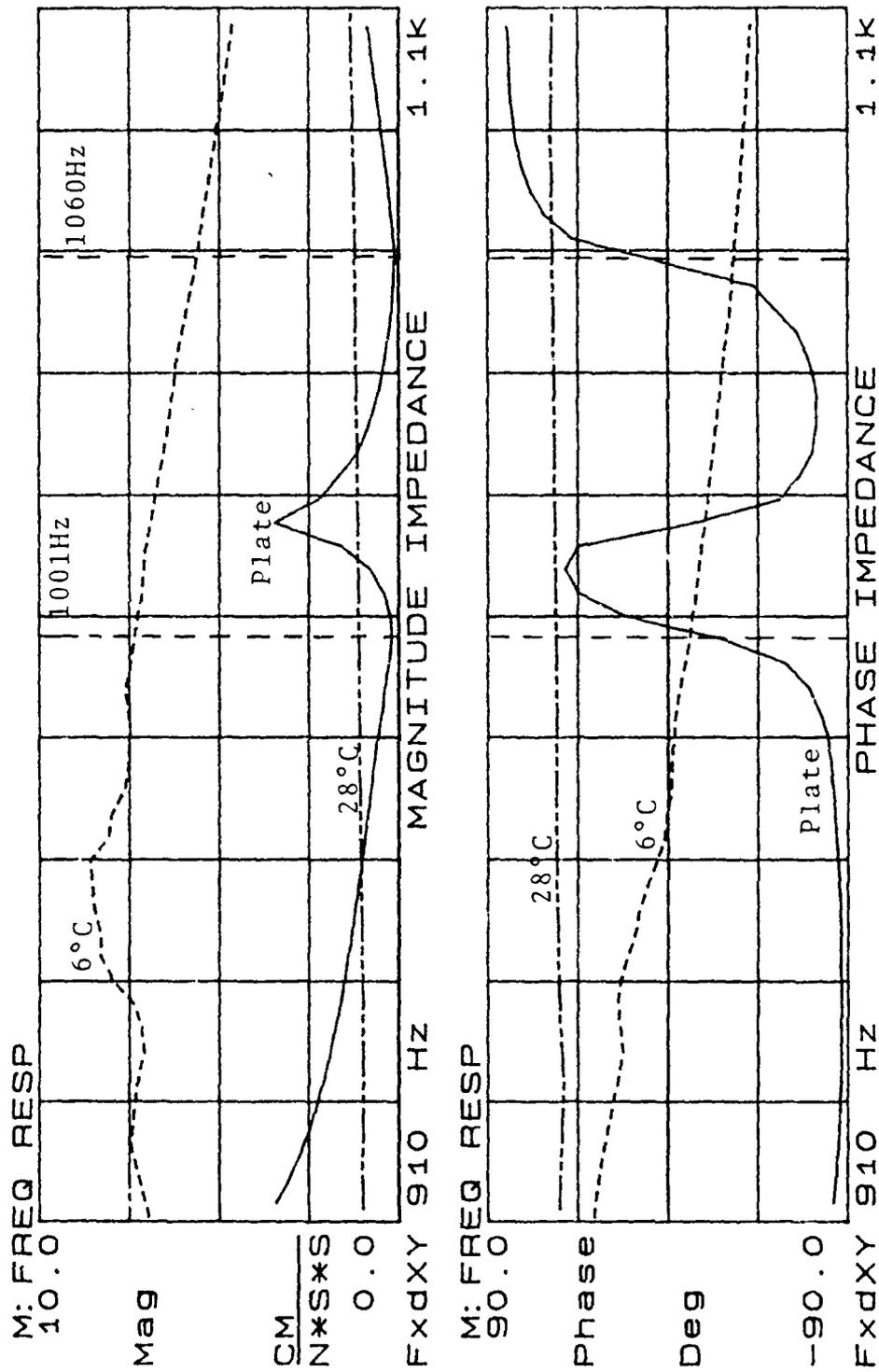
Figure 22. Impedance Matching of the Waveguide Absorber and the Test Plate at location 6J for Resonant Frequencies 1001 Hz and 1060 Hz.

The results of this first waveguide absorber attachment were excellent in that the resonant peaks occurring at 1001 Hz and 1060 Hz were greatly reduced. Figure 23 shows the original undamped response of the plate and the damped response due to the attached absorber for two different temperatures which shows clearly the reduced resonance peaks for the two indicated modes while also showing the better result at the higher temperature due to the improved impedance match. However, the resonant peak at 1824 Hz was still an area of concern due to it's continued prominence as shown in Figure 24.
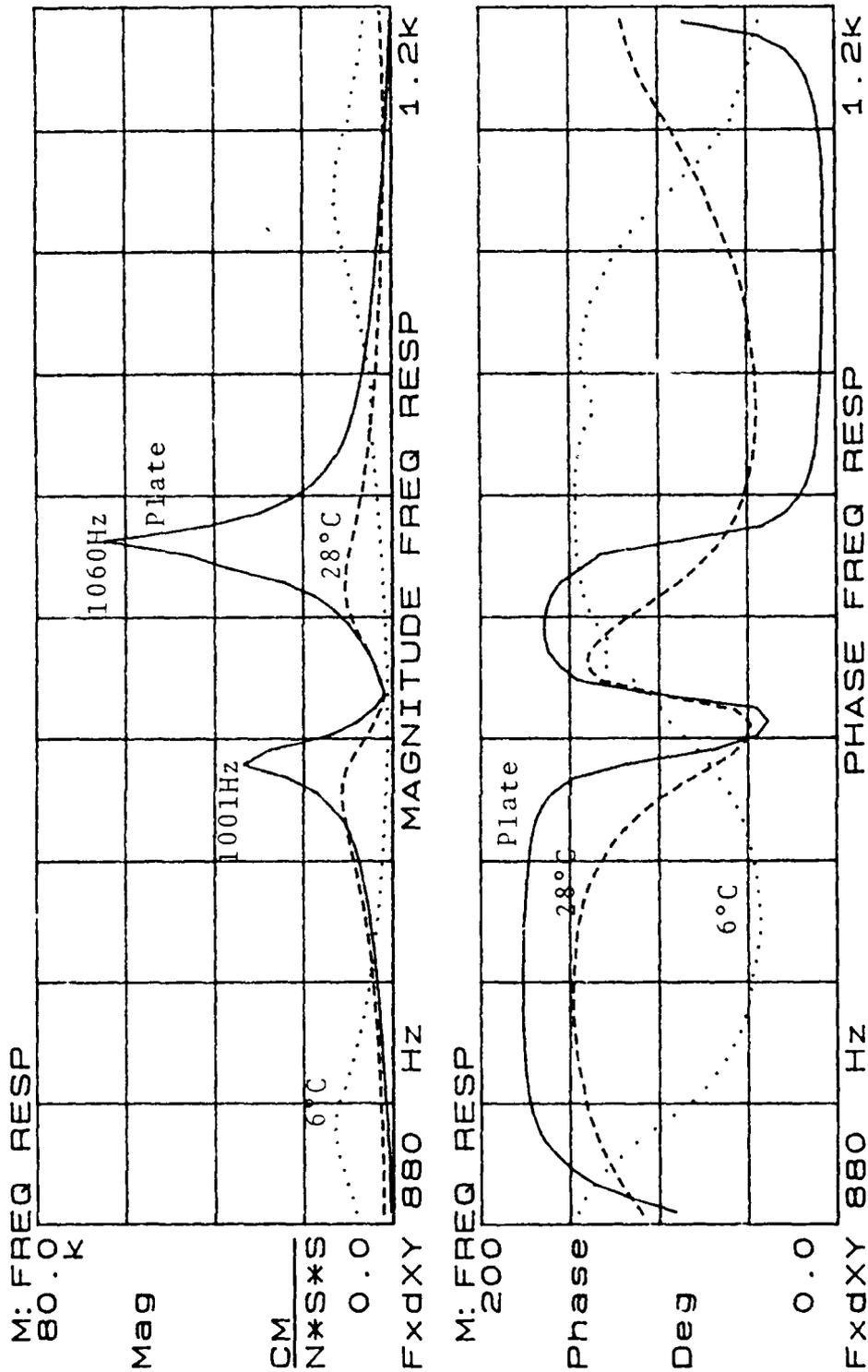
Figure 23. Frequency Response of the Plate. Original Undamped (solid line) versus One 15.2 x 0.953 cm (6 x 0.375 in.) Waveguide Absorber attached at Point 6J at 28° C (82° F) (dashed line) and at 6° C (42° F) (dotted line).
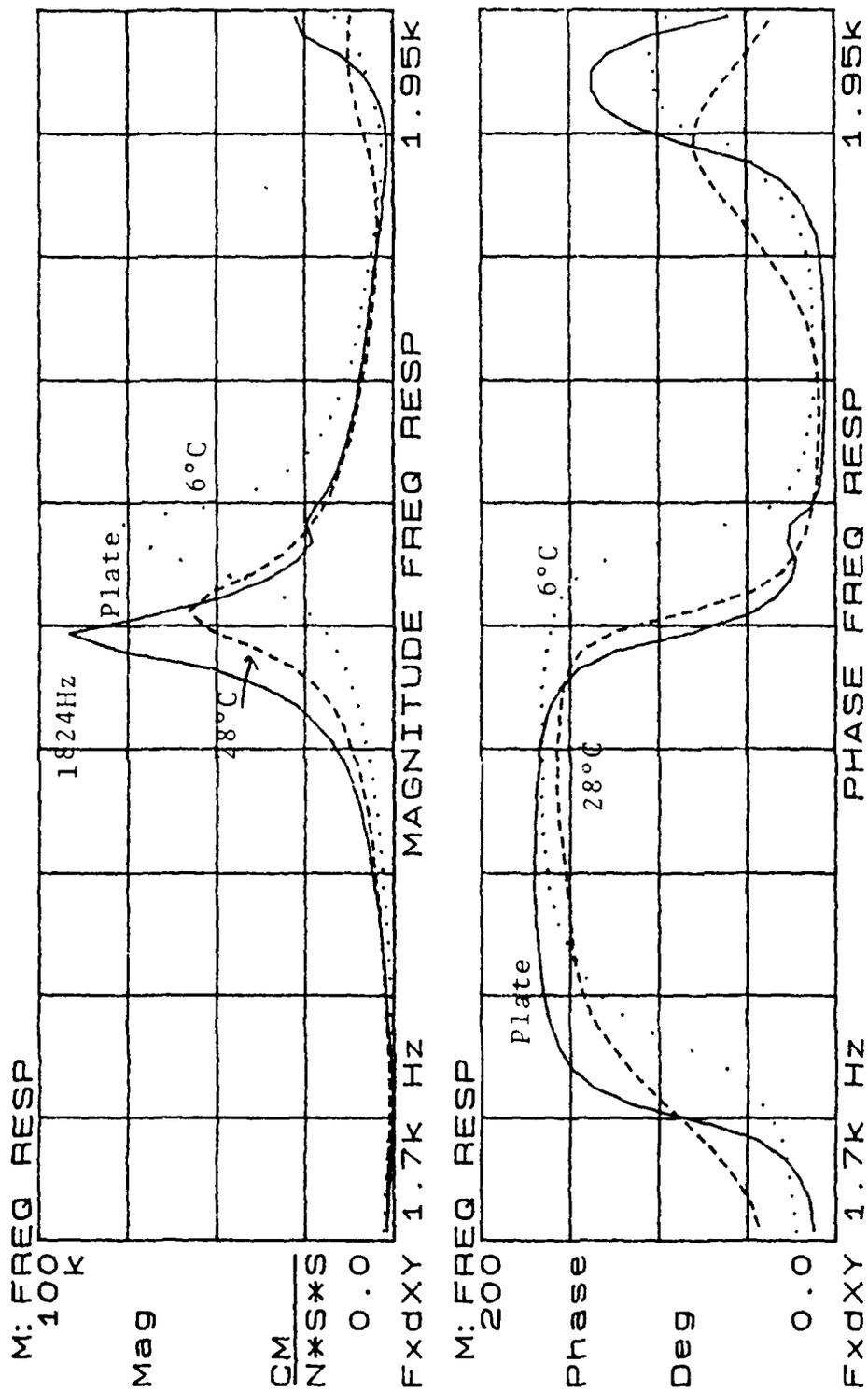
Figure 24. Frequency Response of the Plate. Original Undamped (solid line) versus One 15.2 x 0.953 cm (6 x 0.375 in.) Waveguide Absorber attached at Point 6J at 28° C (82° F) (dashed line) and at 6° C (42° F) (dotted line).

In order to reduce the still prominent 1824 Hz resonant peak, the modal information on the test plate was again reviewed to determine the best possible location for a second waveguide absorber. The theoretical mode for 1945 Hz as shown in Figure 25 was assumed to be related to the actual resonant mode of 1824 Hz and a second waveguide absorber was added to location 2I as shown in Figure 26.
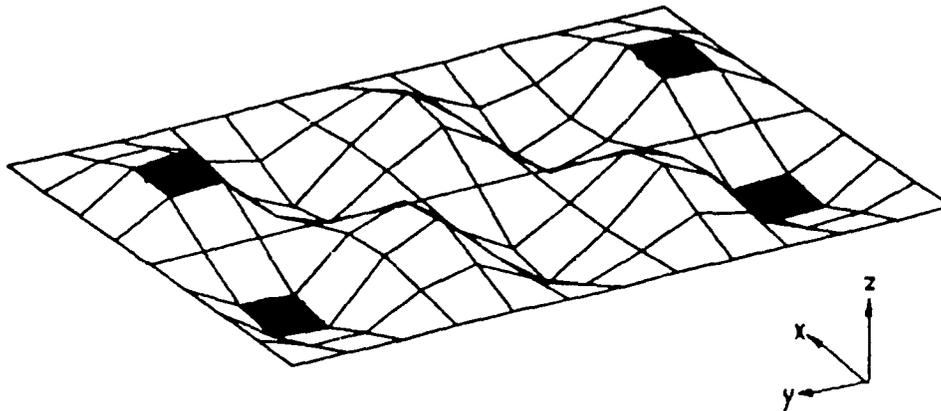
Figure 25. Theoretical Mode 1945 Hz.
(shaded area represents highest motion)
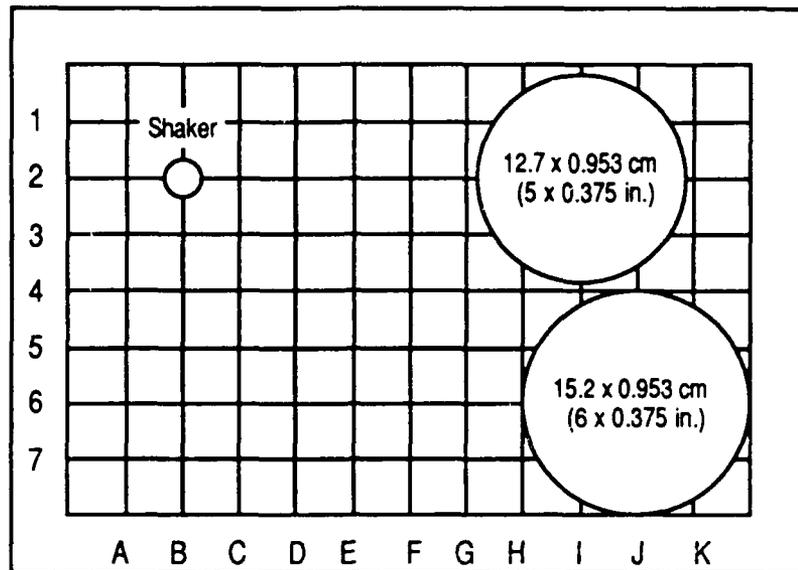
Figure 26. Waveguide Absorbers Mounted on Test Plate.

The resulting frequency response plot for the 1824 Hz resonant peak showed a marked decrease in magnitude. The resonance was still somewhat prominent but had been reduced as shown in Figure 27. To confirm the predicted mounting location of the second waveguide absorber as a correct placement the mount was relocated to 3G, a less prominent anti-node, and the resulting resonant peak at 1824 Hz increased approximately 15% as shown in Figure 28. This confirmed the assumption made earlier that the actual plate mode at 1824 Hz was related to the theoretical mode at 1945 Hz.
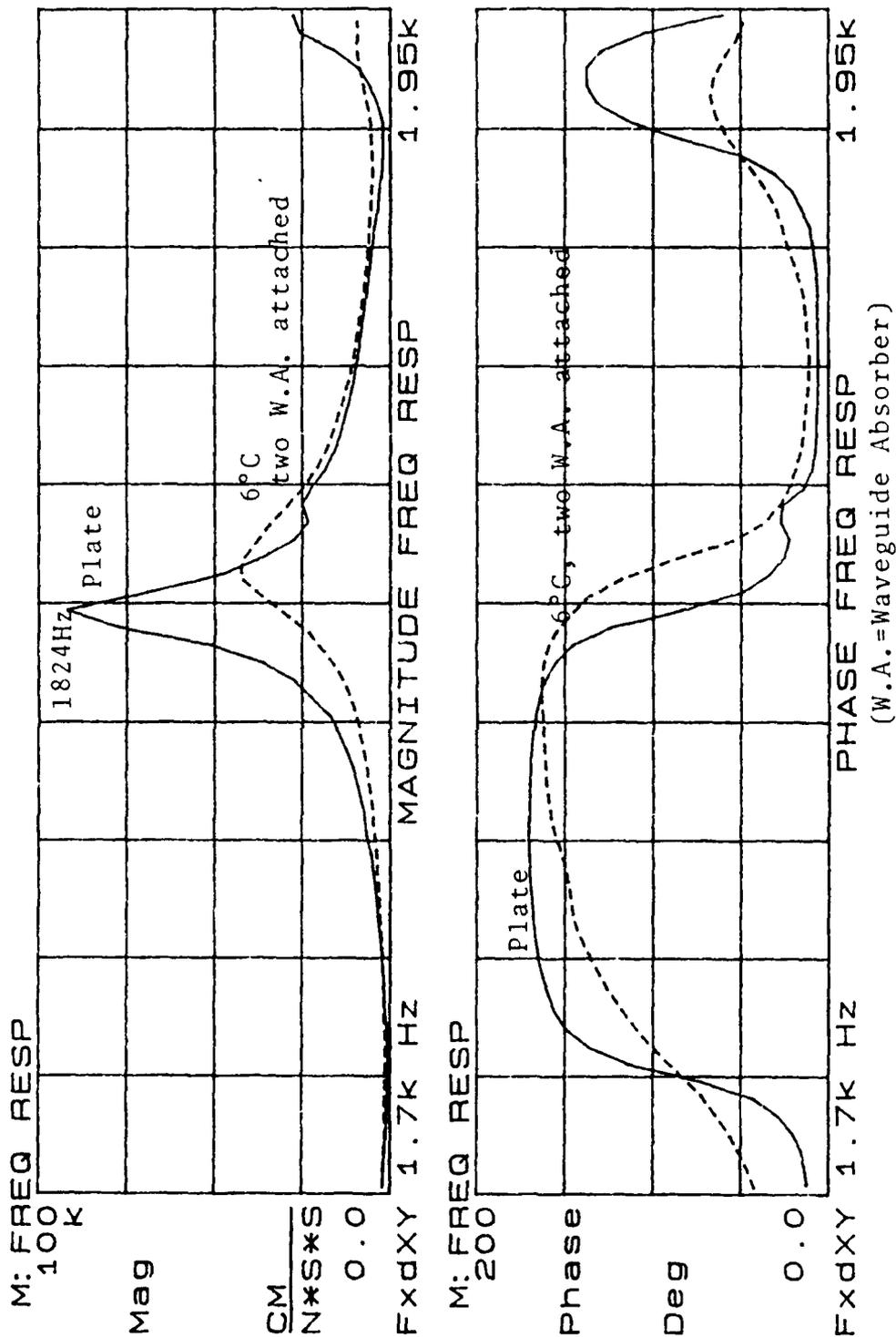
Figure 27. Frequency Response of the Plate. Original Undamped (solid line) versus Two Waveguide Absorbers attached at Points 6J and 2I at 28° C (82° F) (dashed line).
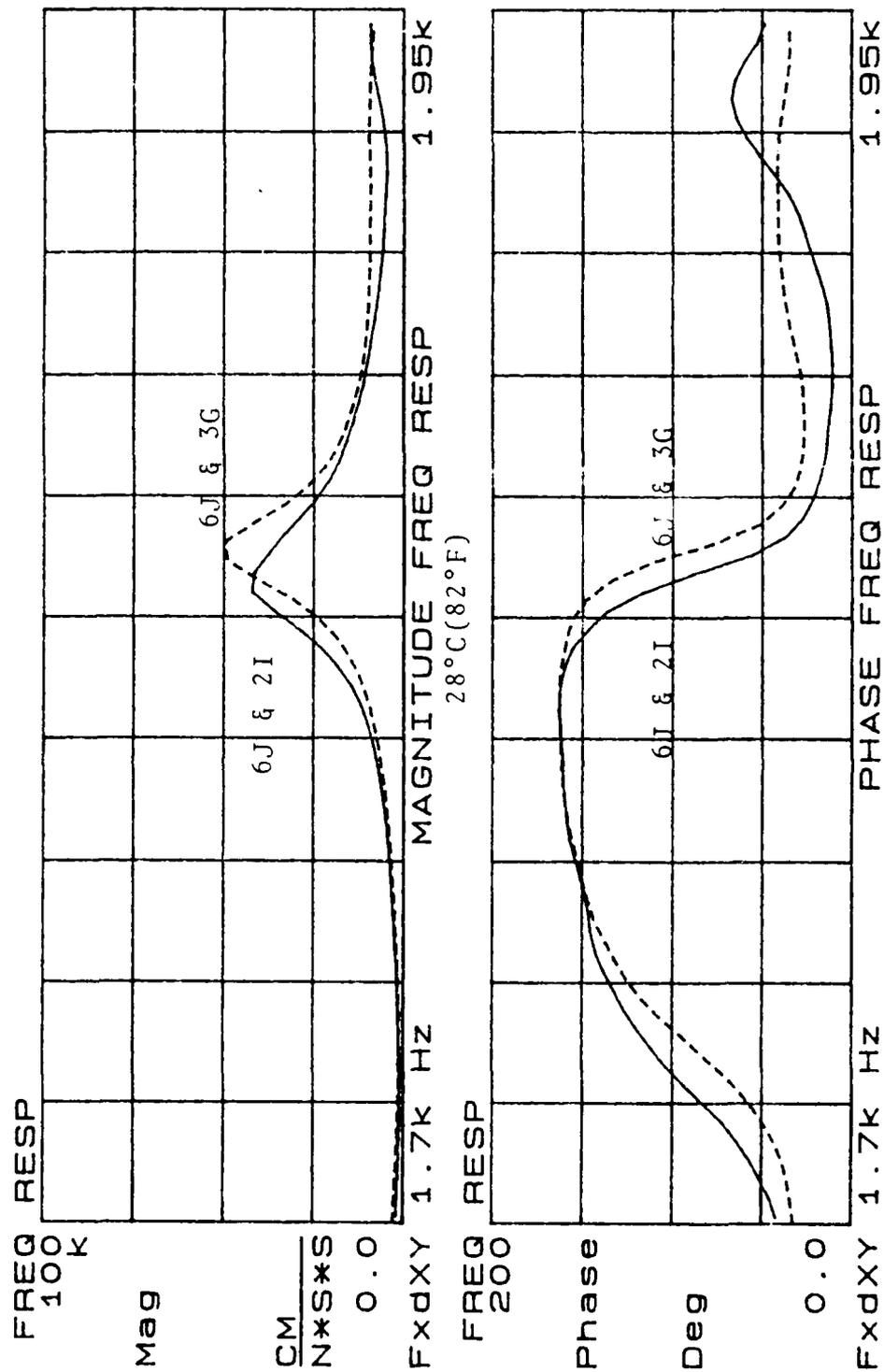
Figure 28. Frequency Response of the Plate with Two Waveguide Absorbers at 28° C (82° F). Original Mounting Location (solid line) versus One Waveguide Absorber shifted from Location 2I to 3G (dashed line).

The resonant peak at 1824 Hz had been reduced approximately 50% by attaching two waveguide absorbers to the plate at selected locations. The other three prominent resonant peaks in the undamped plate were reviewed to ensure that their loss in magnitude had not decreased. Figure 29 shows the resonant frequencies at 1001 Hz, 1060 Hz, and 1388 Hz indicating no reduction in loss magnitude, and possibly some increase resulting from the addition of the second waveguide absorber.
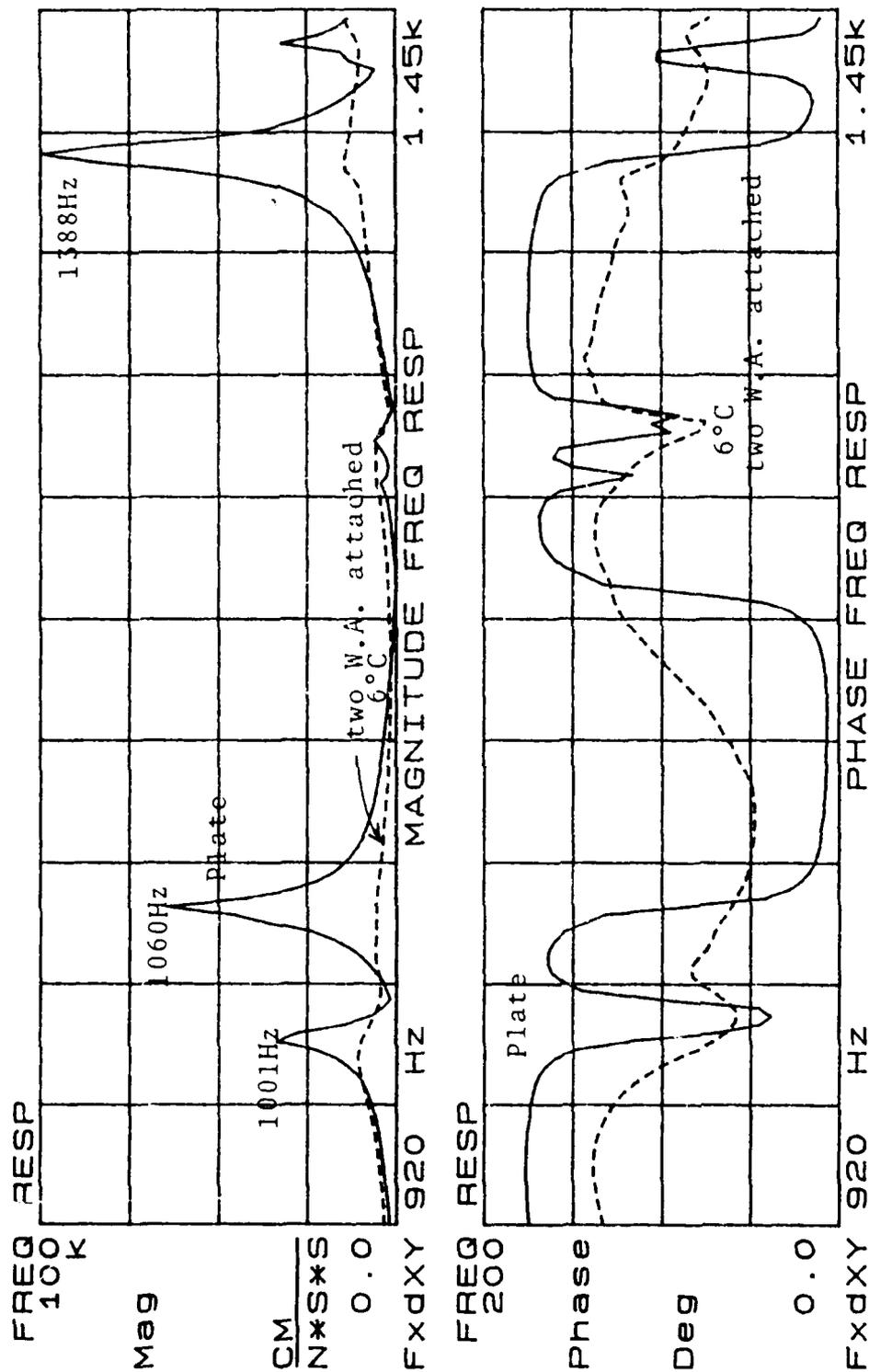
Figure 29. Frequency Response of the Plate with Two Waveguide Absorbers
at 28° C (82° F). Original Undamped Response (solid line) versus Damped
Response (dashed line).

Continuing the goal to reduce the 1824 Hz resonance, the mode information for the plate was reviewed again and a third waveguide absorber was attached to the plate at location 6C as shown in Figure 30.
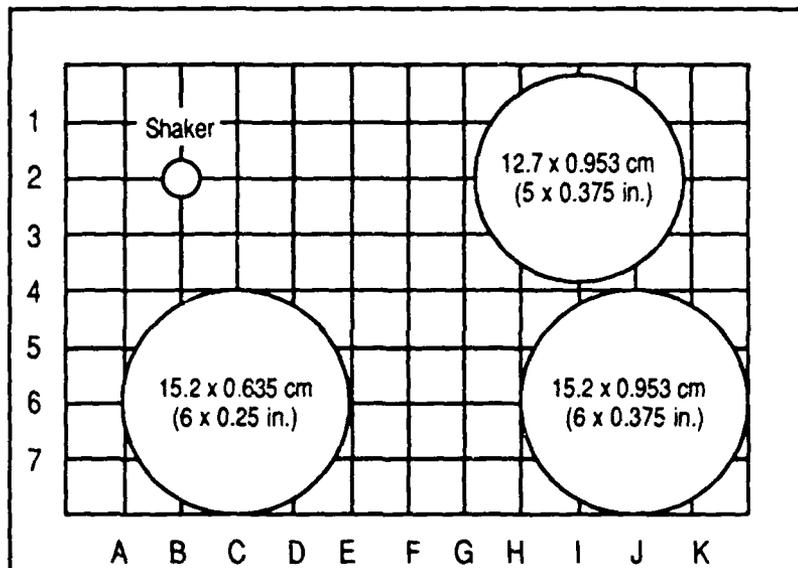
Figure 30. Waveguide Absorbers Mounted on Test Plate.

The resulting frequency response plot again showed a clear decrease in the 1824 Hz resonant frequency magnitude of the test plate. Additionally, the other resonant frequency magnitudes were still maintained at a significantly reduced level. The addition of the third waveguide absorber resulted in a reduction of the 1824 Hz resonant peak of greater than 60% as shown in Figure 31.

An overall plot of the frequency response of the damped plate from 0-2k Hz is shown in figure 32. Additionally, a db plot of displacement over force is also shown in figure 33. This plot clearly shows the marked decrease in frequency response of, in some areas, greater than 10db.
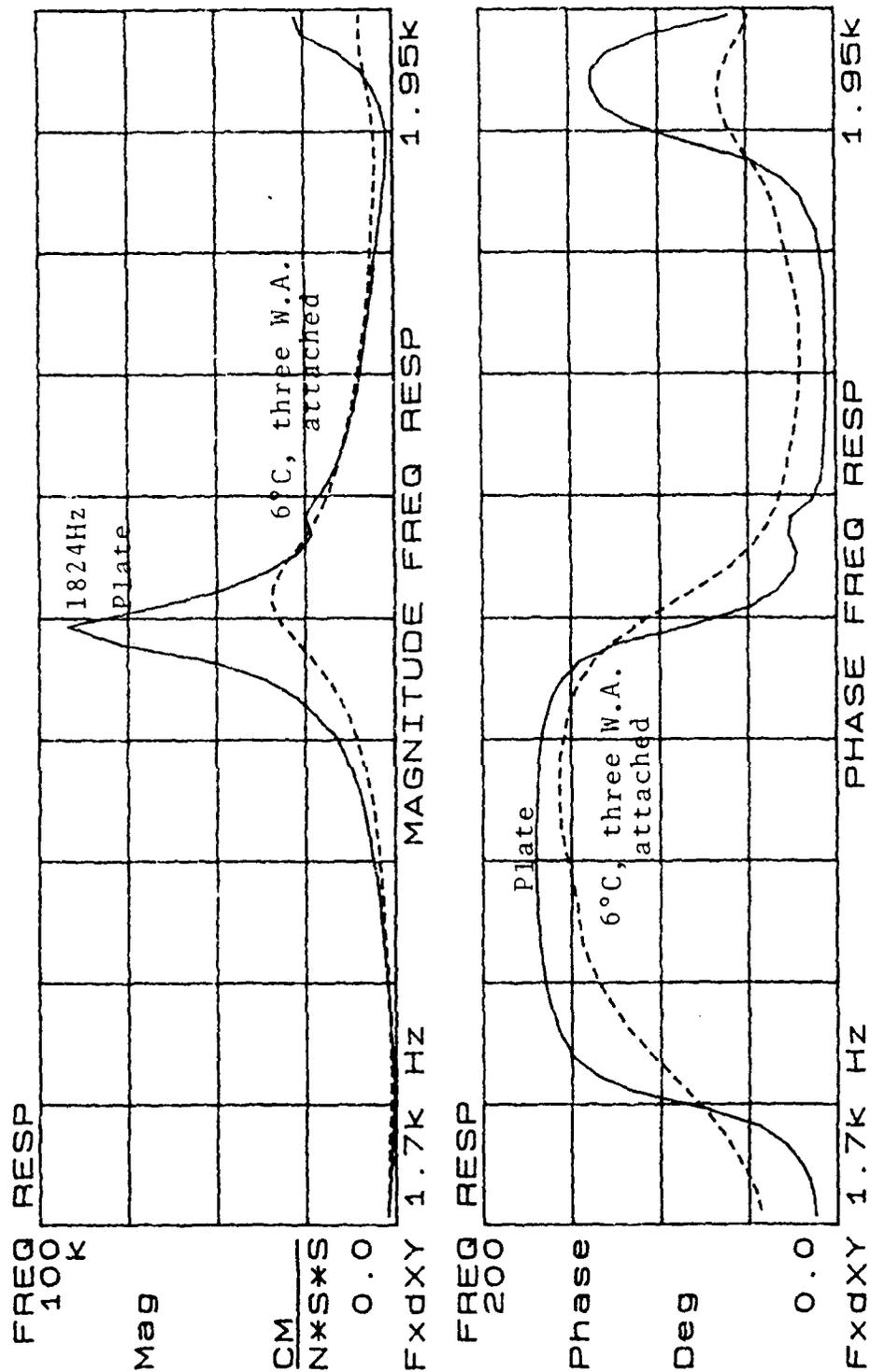
Figure 3L Frequency Response of the Plate with Three Waveguide Absorbers at 28° C (82° F) at the 1824 Hz resonance. Original Undamped Response (solid line) versus Damped Response (dashed line).
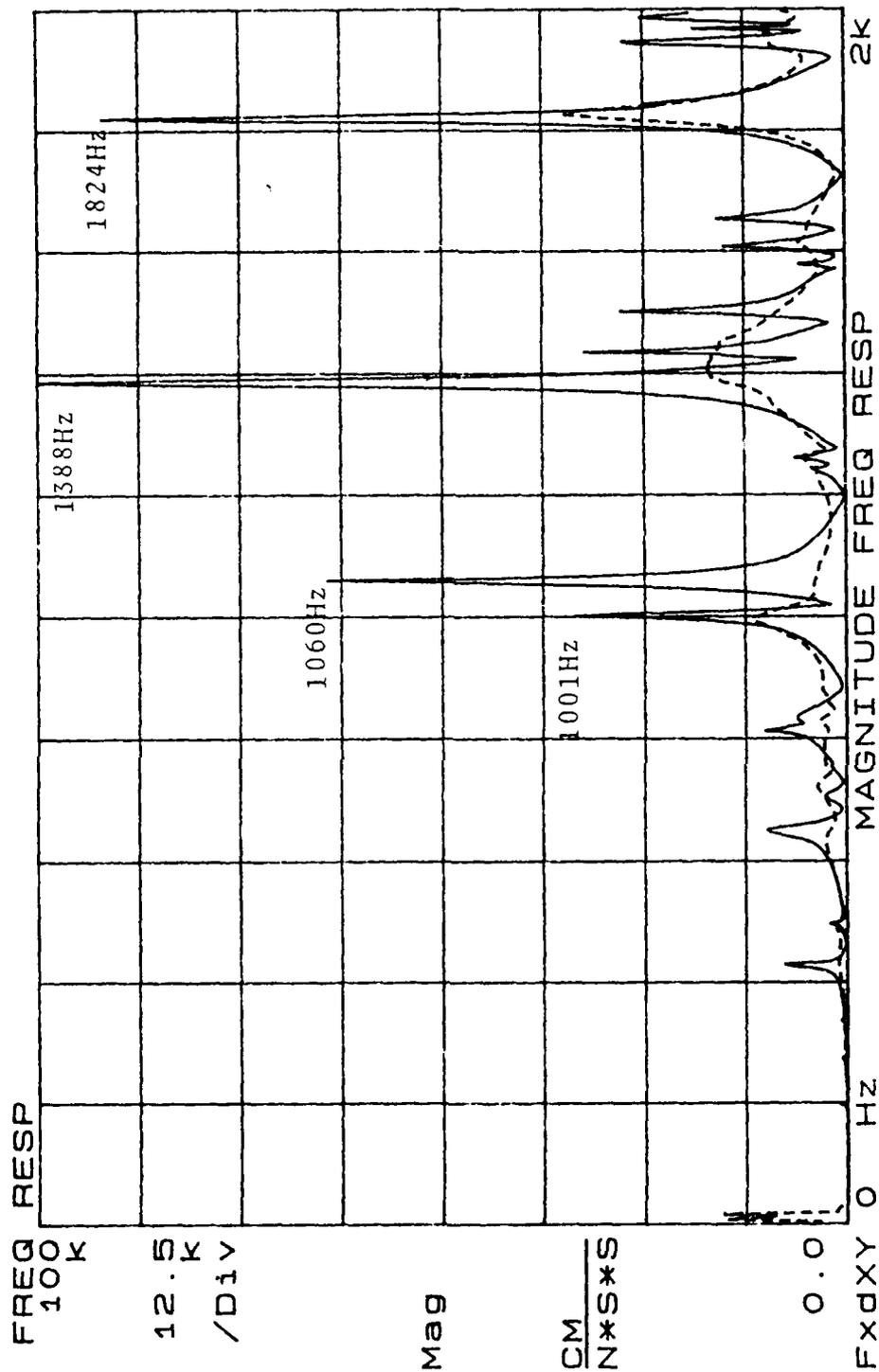
Figure 32. Frequency Response of the Plate with Three Waveguide Absorbers at 28° C (82° F) from 0-2k Hz. Original Undamped Response (solid line) versus Damped Response (dashed line).
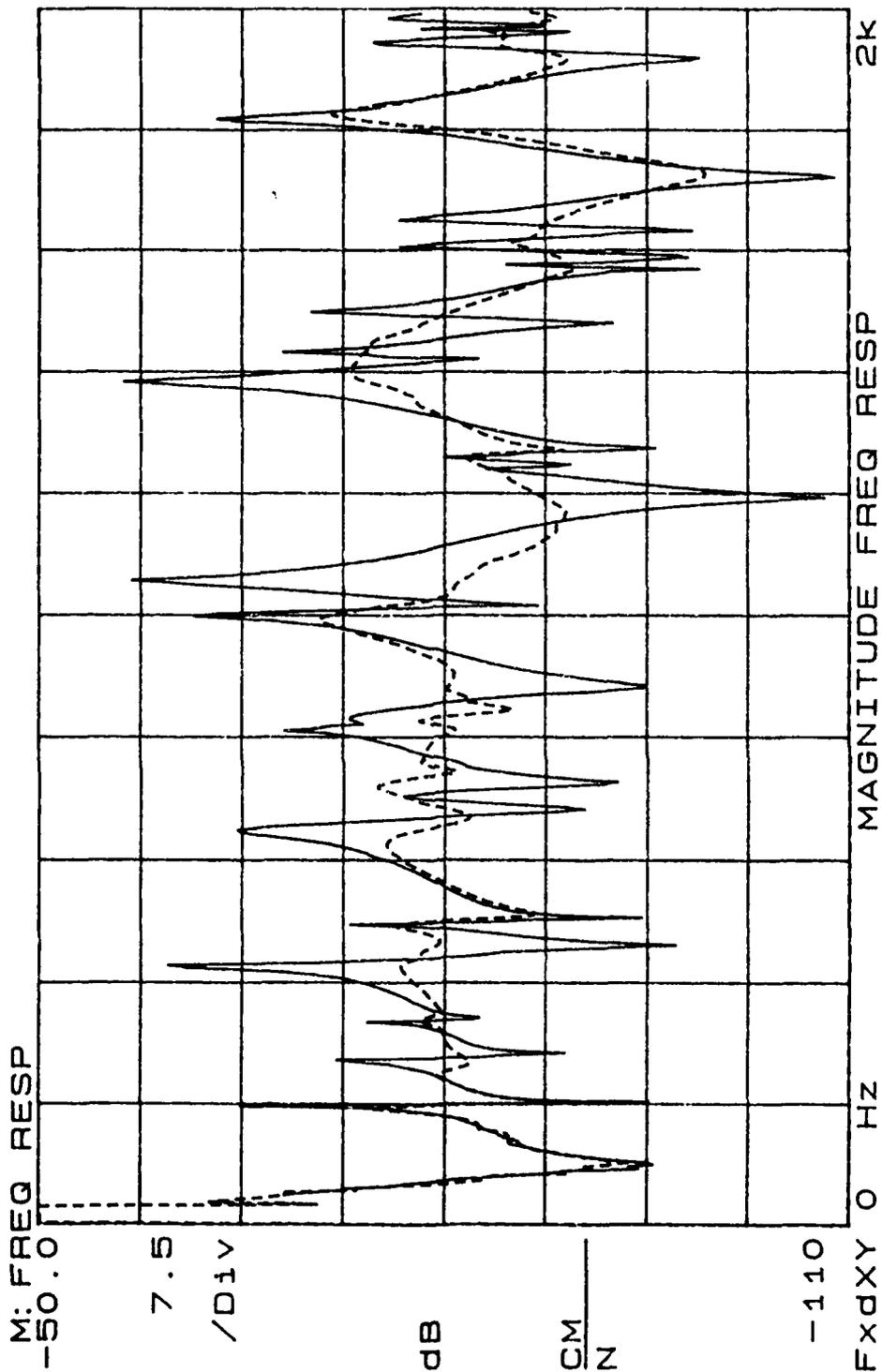
Figure 33. Frequency Response (displacement over force) of the Plate in
dB scale with Three Waveguide Absorbers at 28° C (82° F). Original
Undamped Response (solid line) versus Damped Response (dashed line).

V. CONCLUSIONS

Experimental studies have shown that the computer prediction model is very good in calculating the impedance of the viscoelastic waveguide absorber. The error in the comparison of the experimental data and the predicted data was possibly due to the material characteristics data used in the computer program.

The viscoelastic waveguide absorber effectiveness proved very sensitive to mounting location on the test plate and impedance matching with the plate mount location.

Experimental studies show a single viscoelastic waveguide absorber is very effective in suppressing resonances in wide frequency bands. Additionally, multiple viscoelastic waveguide absorbers are very effective in additive vibration reduction for a given frequency range.

A. REDUCING VIBRATIONS IN ANY PLATE

There are many methods of reducing the noise and vibrations in a structure. However, few are as simple to apply as the waveguide absorber method. There are three steps to reducing structural vibrations with this method. The first step is to determine the undesirable resonant frequencies of the structure. This step is usually the easiest in the procedure depending upon the chosen method.

The second step is to determine the structure locations which have the greatest vibrational motion for the particular frequencies which are undesirable. This will likely be the most difficult step. A finite element analysis using a computer can easily determine the nodes, and more importantly, the anti-nodes for the frequencies of interest. However, the

most reliable method would be to conduct experimental studies on the actual structure by modal testing which, if located inside a ship, could be difficult depending on the structure location and the amount of space surrounding it. A finite element computer analysis can also be performed with the level of difficulty proportional to the level of complication in the structural shape.

The third step in the waveguide damping method would be to match the impedances of the structure locations with the waveguide absorbers. The average operating temperature of the environment surrounding the structure now becomes very important since the viscoelastic material is very sensitive to temperature changes and the resulting impedances will vary with the temperature.

The final application of the waveguide to the structure should be considerably easier than other damping methods since the waveguide can simply be stud welded to the structure as opposed to gluing large damping sheets to a structure. Once the waveguides are attached, the actual waveguide absorber can be changed to match the changing environment if necessary. This ability provides a unique adaptability which no other damping method can provide as easily.

VI. RECOMMENDATIONS FOR FURTHER STUDY

Based upon the results of this experimental study, the following recommendations should be considered for continuing studies in this field.

1. In this study, large thin circular viscoelastic waveguide absorbers were not tested thoroughly at high temperatures (above 28° C / 82° F) since the large disk tended to sag down and contact the test plate. This difficulty might be overcome by incorporating constrained layer waveguide absorbers or using materials more resistant to temperature changes.

2. The next step involving waveguide absorbers might include developing optimization computer software to predict ideal mounting locations for waveguide absorbers. The software would produce not only the mounting location for the absorber, but also the best viscoelastic waveguide absorber size to use for a situation.

APPENDIX   A.

## EXPERIMENTAL VISCOELASTIC WAVEGUIDE
ABSORBER IMPEDANCE
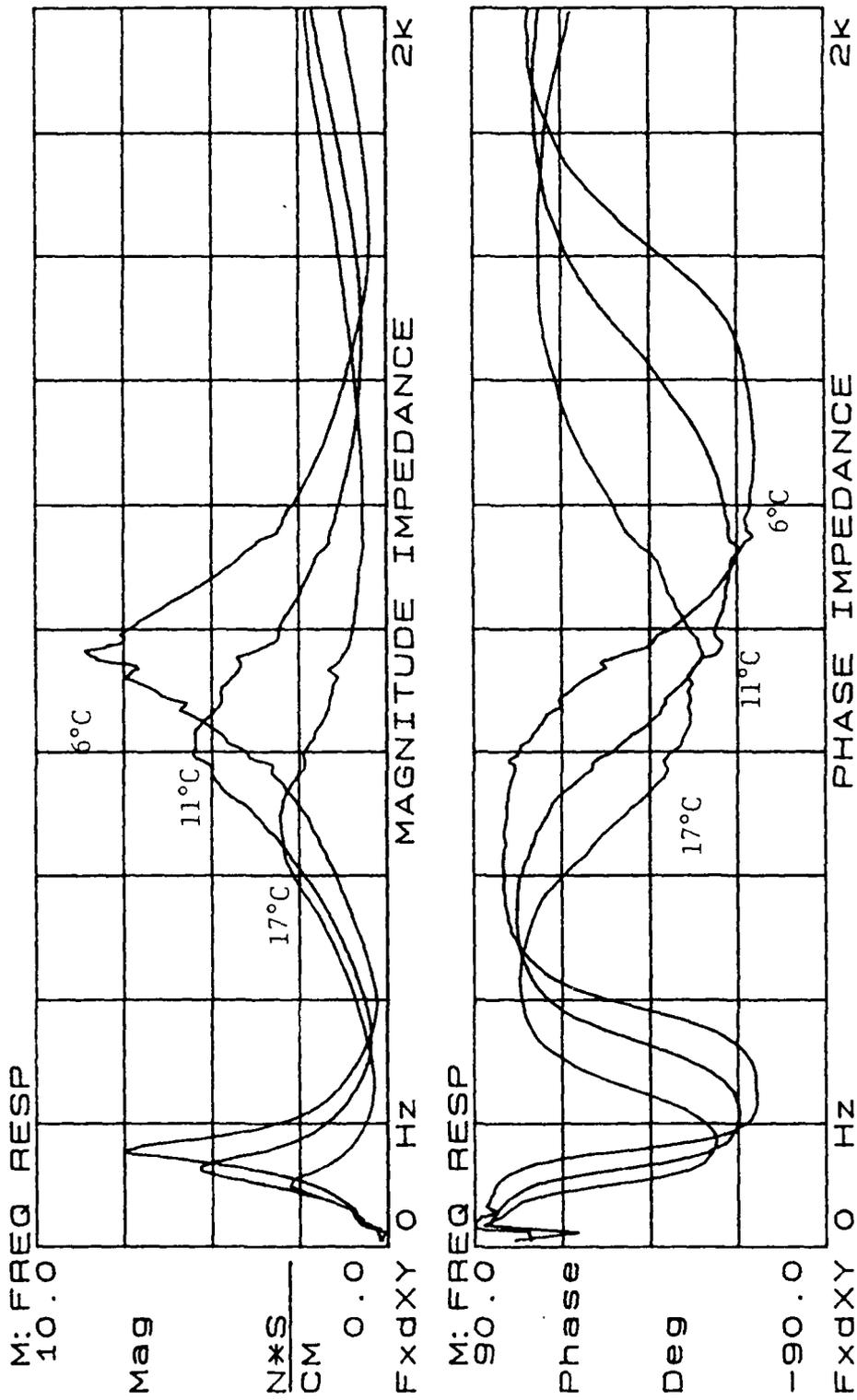
Figure 34. 15.2 x 0.953 cm (6 x 0.375 in.) Viscoelastic Waveguide Absorber

Impedance Trend for Temperatures from 6° C (42° F) to 17° C (62° F).
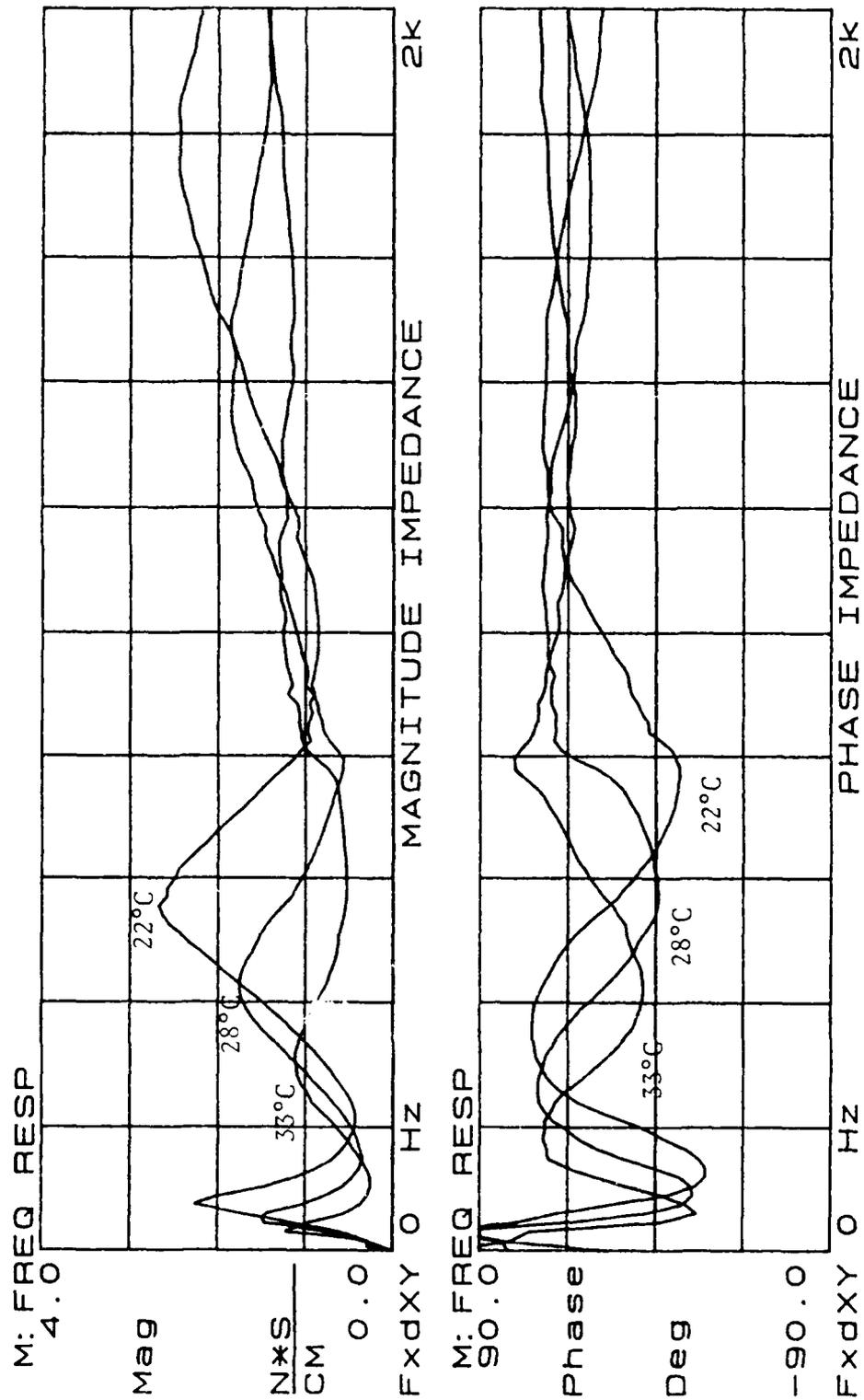
Figure 35. 15.2 x 0.953 cm (6 x 0.375 in.) Viscoelastic Waveguide Absorber

Impedance Trend for Temperatures from 22° C (72° F) to 33° C (92° F).
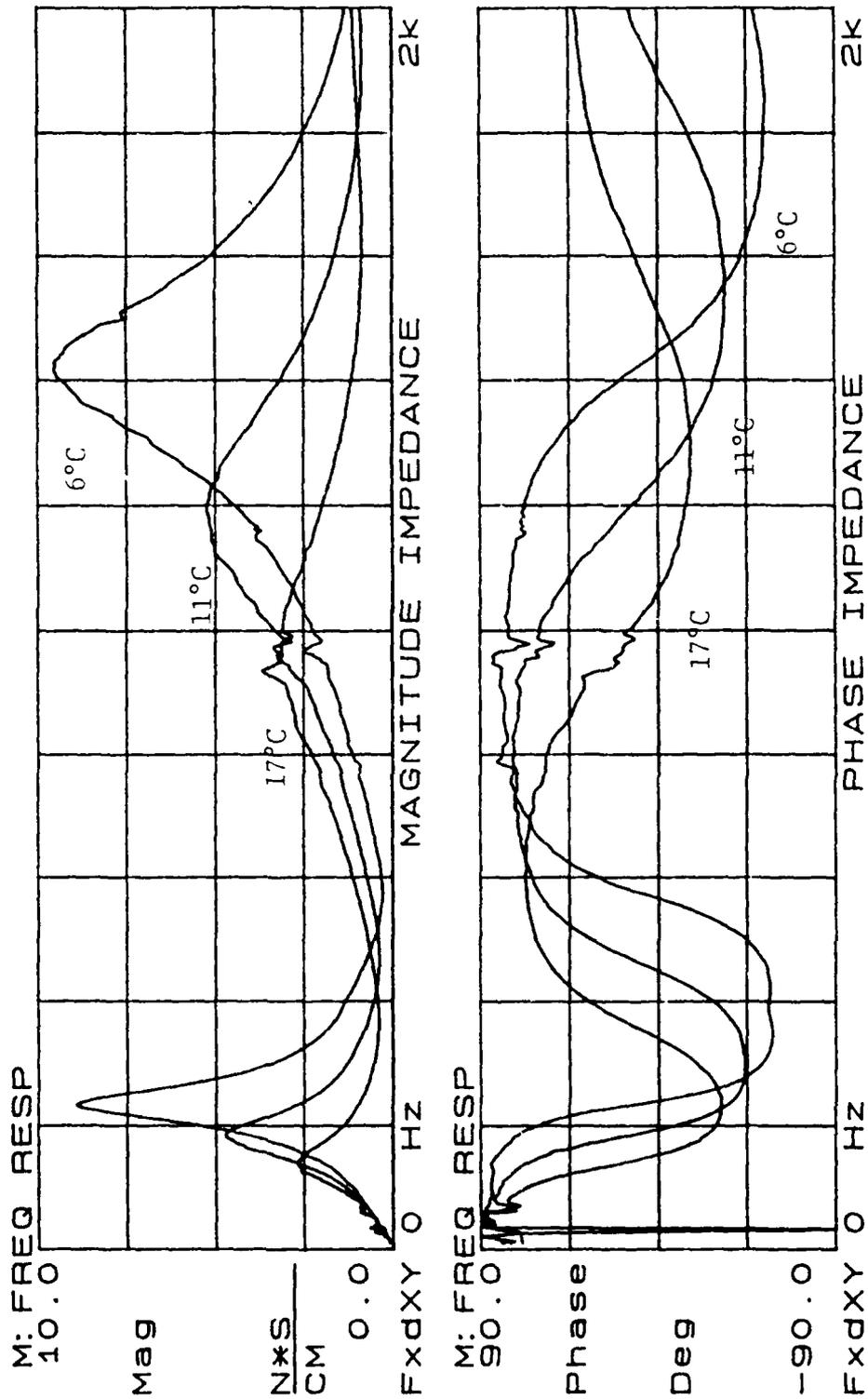
Figure 36. 12.7 x 0.953 cm (5 x 0.375 in.) Viscoelastic Waveguide Absorber

Impedance Trend for Temperatures from 6° C (42° F) to 17° C (62° F).
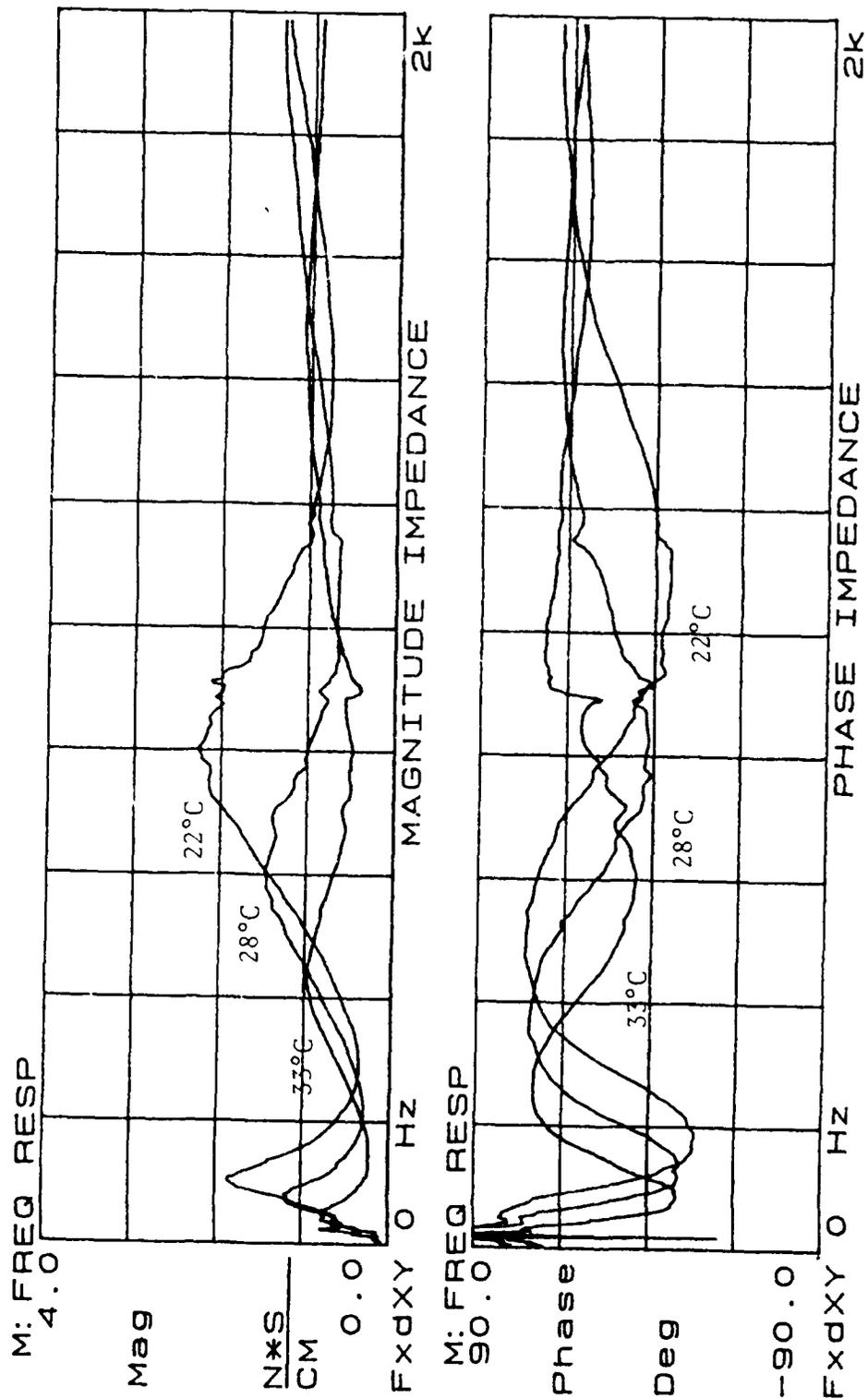
Figure 37. 12.7 x 0.953 cm (5 x 0.375 in.) Viscoelastic Waveguide Absorber

Impedance Trend for Temperatures from 22° C (72° F) to 33° C (92° F).
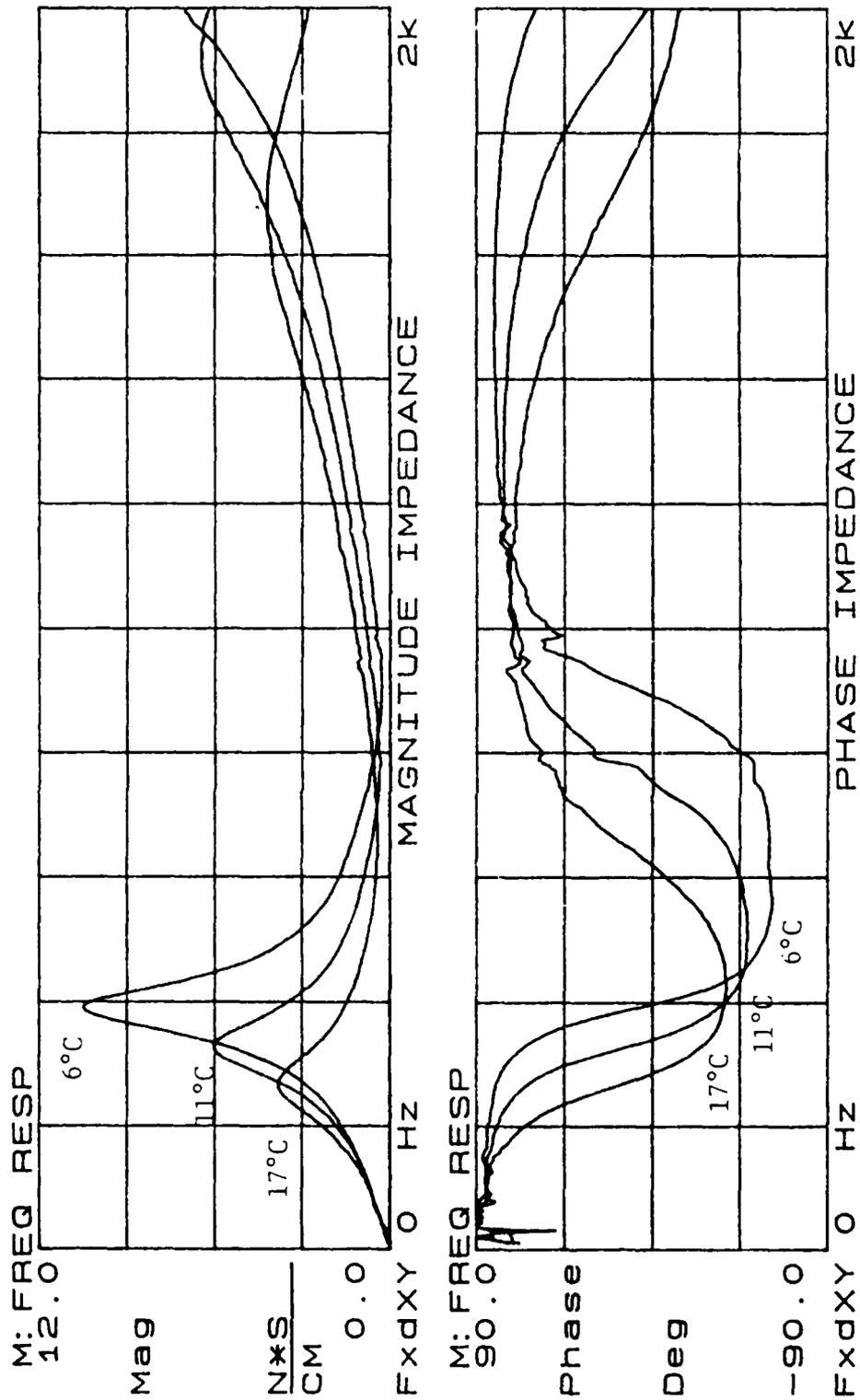
Figure 38. 10.2 x 0.953 cm (4 x 0.375 in.) Viscoelastic Waveguide Absorber
Impedance Trend for Temperatures from 6° C (42° F) to 17° C (62° F).
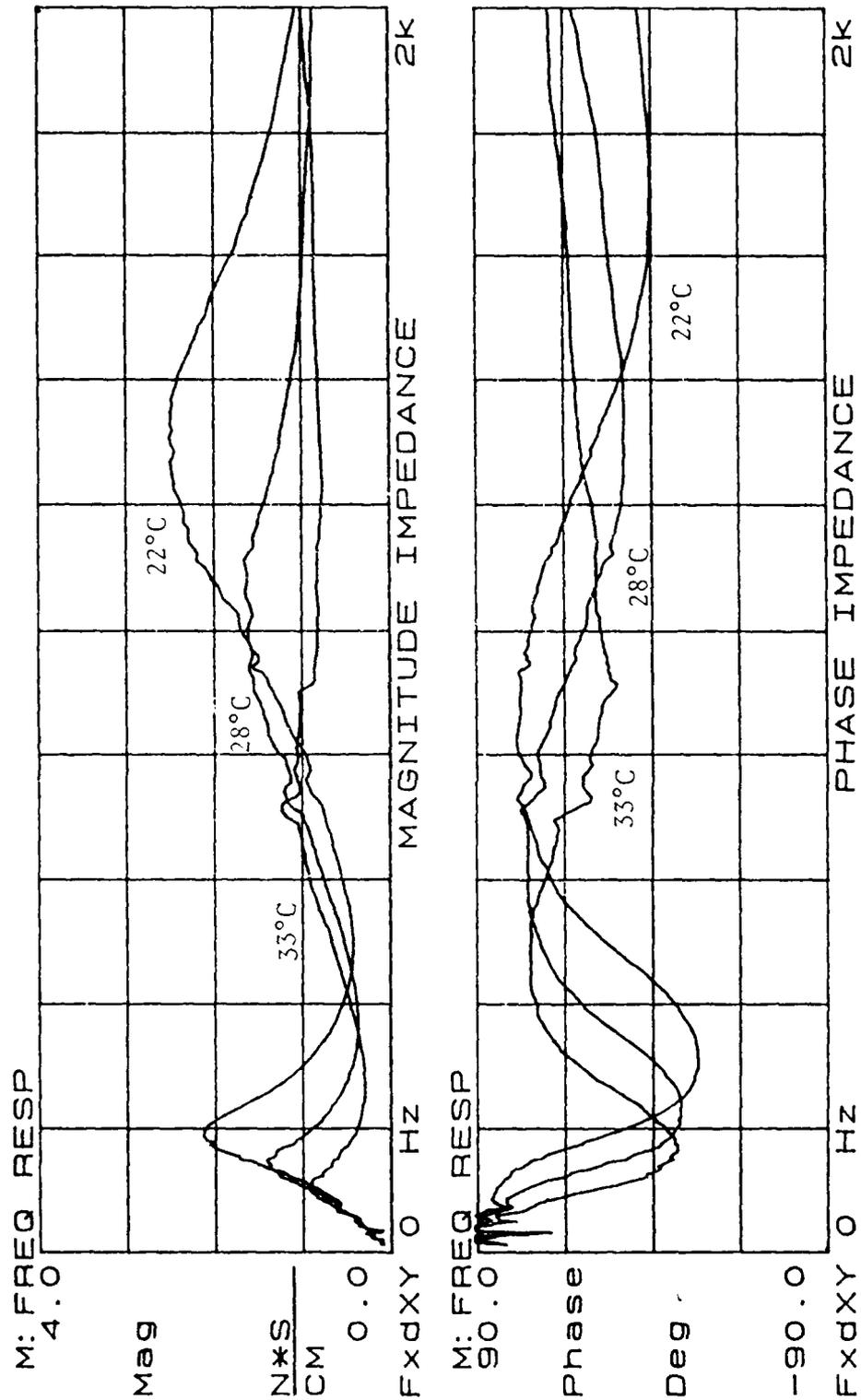
Figure 39. 10.2 x 0.953 cm (4 x 0.375 in.) Viscoelastic Waveguide Absorber Impedance Trend for Temperatures from 22° C (72° F) to 33° C (92° F).
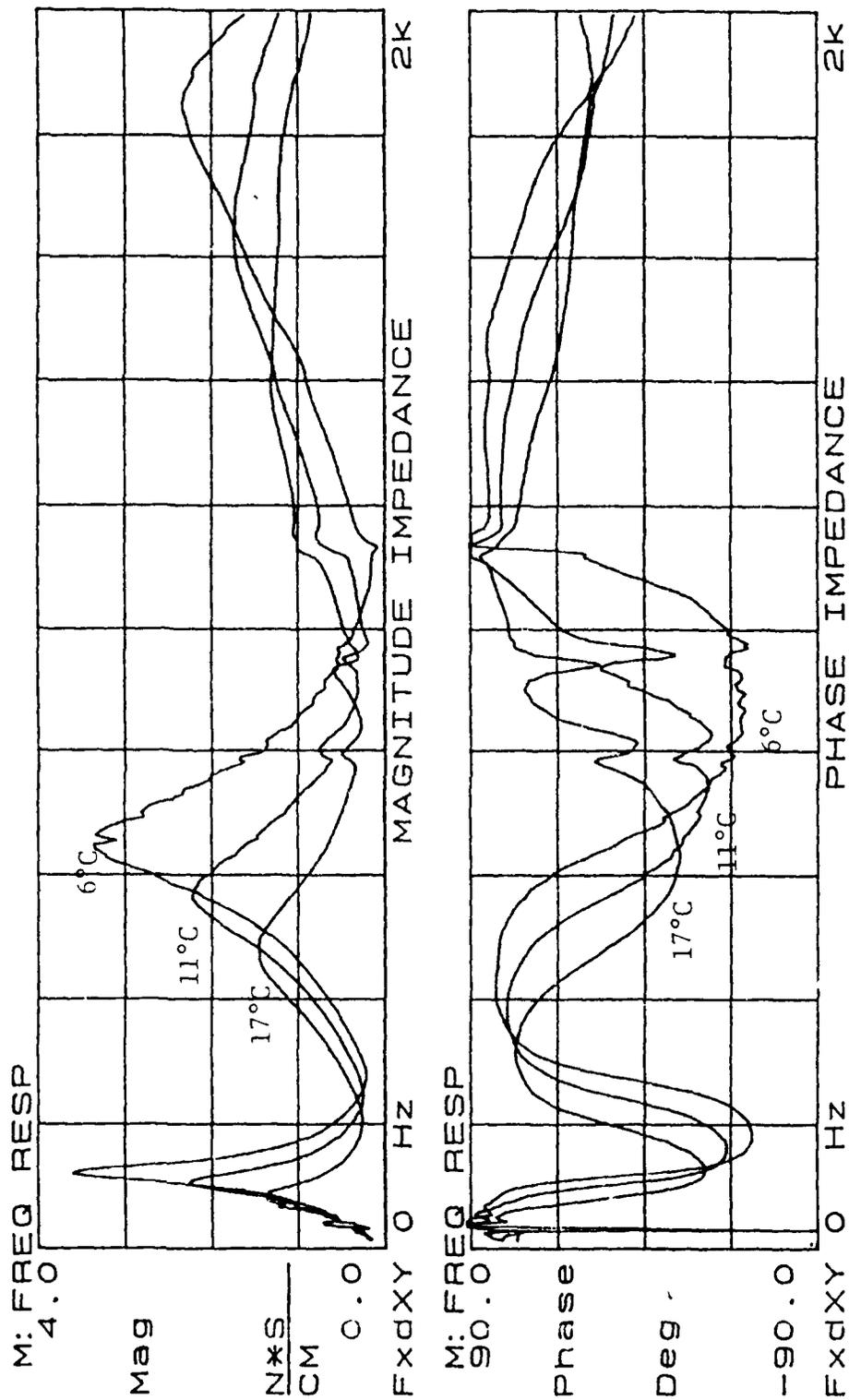
Figure 40. 15.2 x 0.635 cm (6 x 0.25 in.) Viscoelastic Waveguide Absorber

Impedance Trend for Temperatures from 6° C (42° F) to 17° C (62° F).
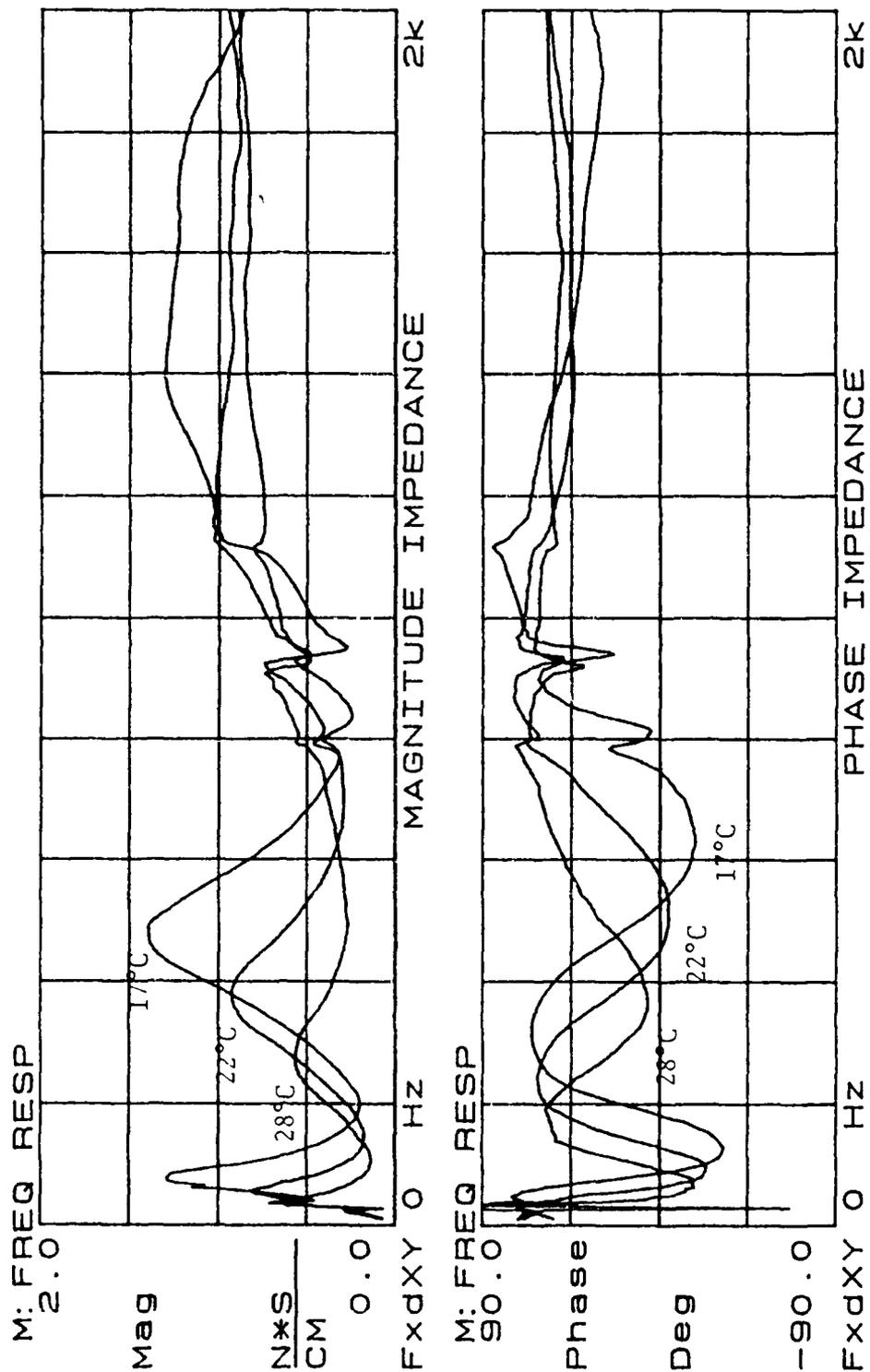
Figure 41. 15.2 x 0.635 cm (6 x 0.25 in.) Viscoelastic Waveguide Absorber
Impedance Trend for Temperatures from 17° C (62° F) to 28° C (82° F).
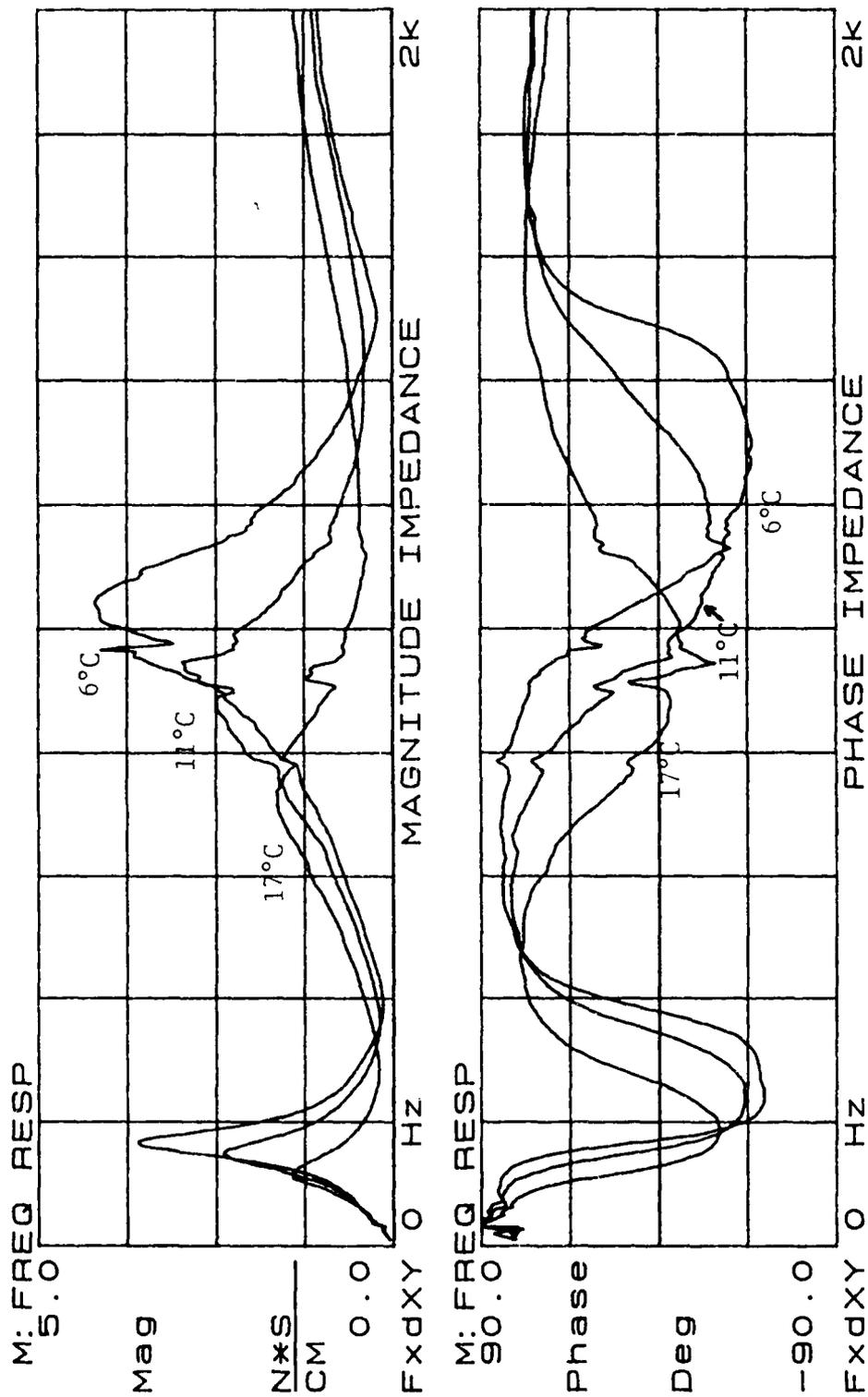
Figure 42. 12.7 x 0.635 cm (5 x 0.25 in.) Viscoelastic Waveguide Absorber Impedance Trend for Temperatures from 6° C (42° F) to 17° C (62° F).
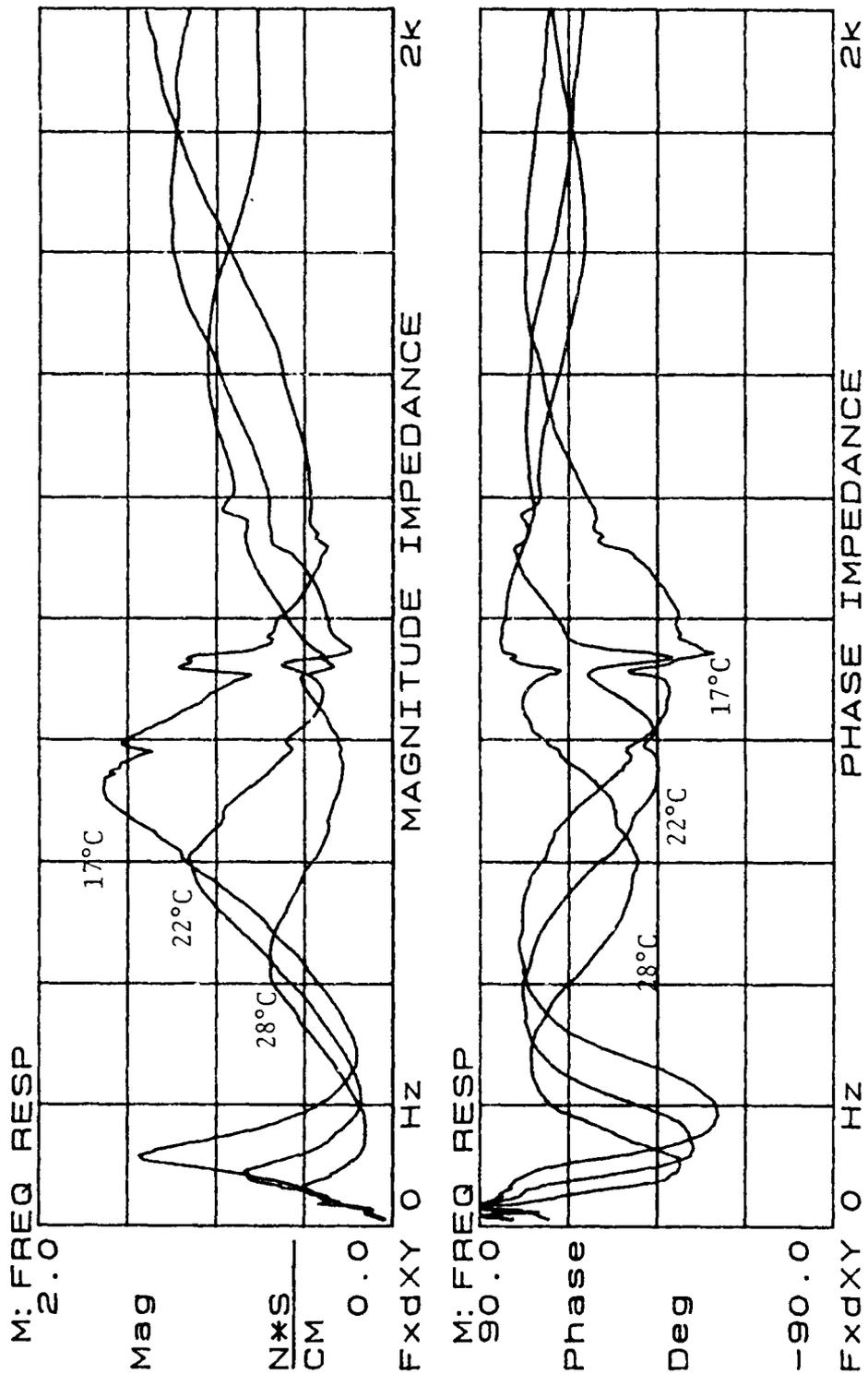
Figure 43. 12.7 x 0.635 cm (5 x 0.25 in.) Viscoelastic Waveguide Absorber

Impedance Trend for Temperatures from 17° C (62° F) to 28° C (82° F).

60
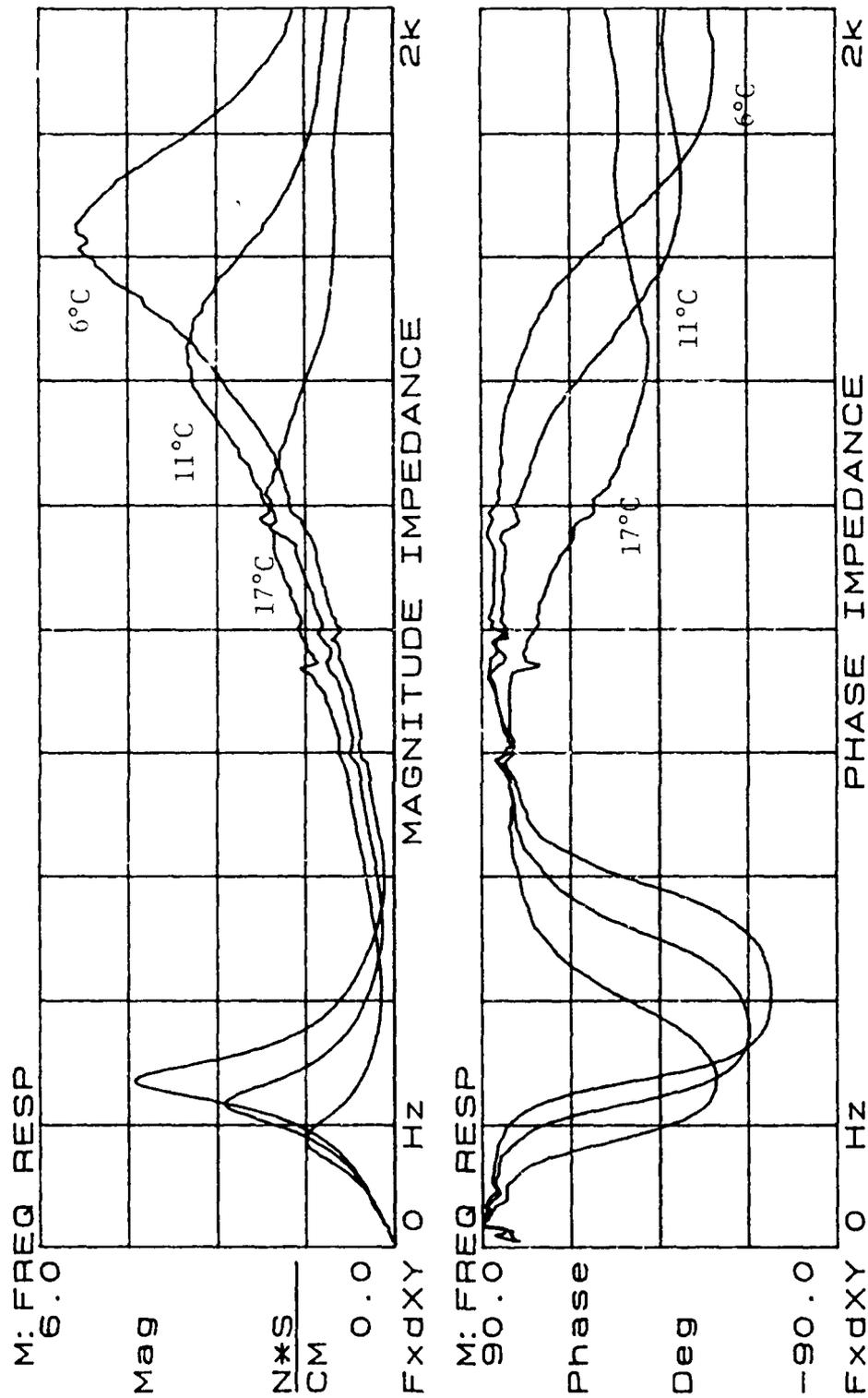
Figure 44. 10.2 x 0.635 cm (4 x 0.25 in.) Viscoelastic Waveguide Absorber
Impedance Trend for Temperatures from 6° C (42° F) to 17° C (62° F).

61
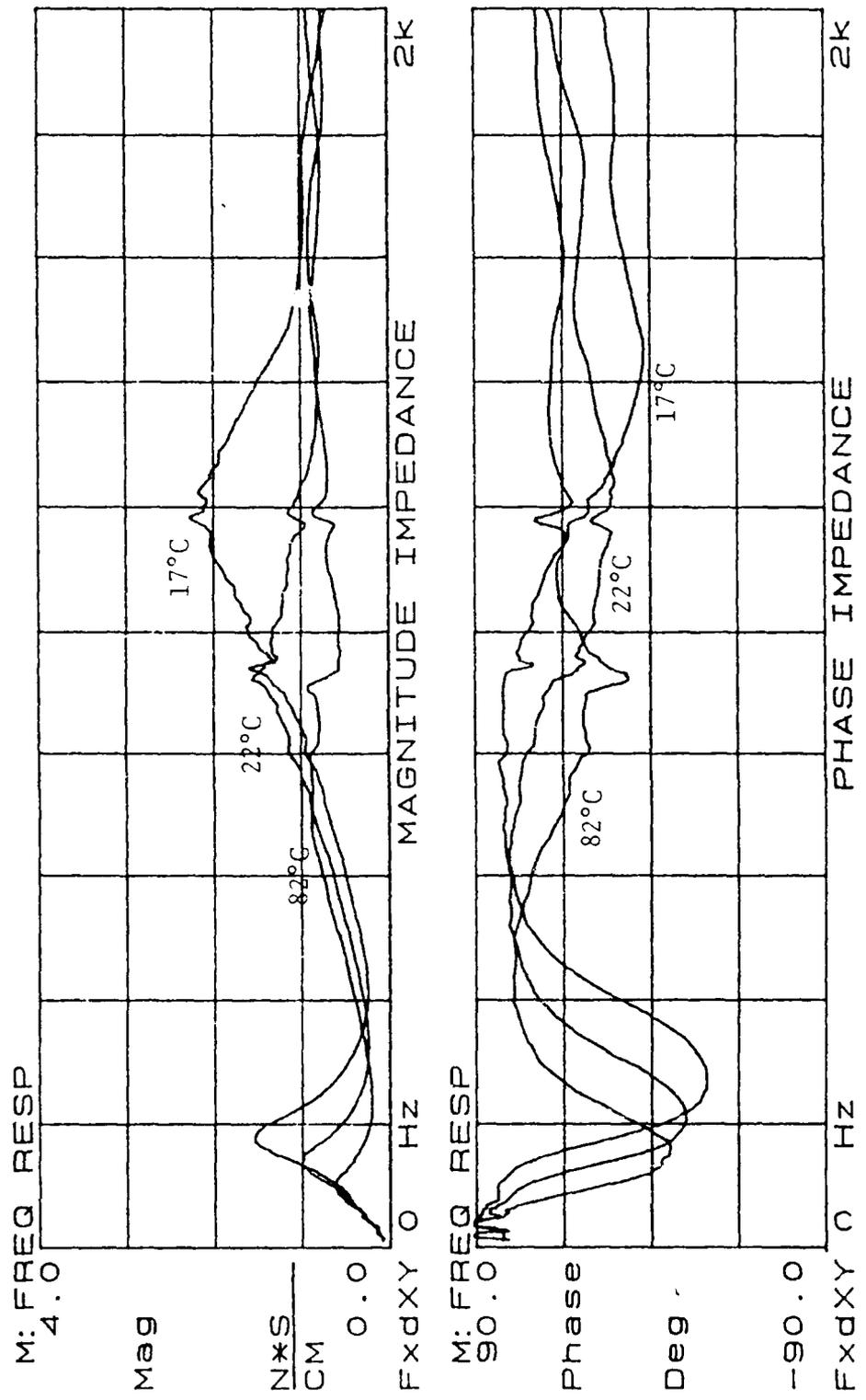
Figure 45. 10.2 x 0.635 cm (4 x 0.25 in.) Viscoelastic Waveguide Absorber
Impedance Trend for Temperatures from 17° C (62° F) to 28° C (82° F).

LIST OF REFERENCES

1. Ungar, E. E. and Kurzweil, L. G., <u>Preliminary Evaluation of Waveguide Vibration Absorbers</u>, Flight Dynamics Laboratory, Air Force Wright Aeronautical Laboratories Report AFWAL-TR-83-3125 Jan. 1984.

2. Lee, G.G., <u>Analytical and Experimental Studies of Beam Waveguide Absorbers for Structural Damping</u>, Masters Thesis, Naval Postgraduate School, Monterey, CA, Mar. 1988.

3. Horne, C.T., <u>Passive Vibration Control Using Viscoelastic and Constrained Layer Beam Waveguide Absorbers</u>, Masters Thesis, Naval Postgraduate School, Monterey, CA, Sep. 1988.

4. Hettema, C.D., <u>The Modeling of Viscoelastic Circular Plates for use as Waveguide Absorbers</u>, Masters Thesis, Naval Postgraduate School, Monterey, CA, Sep. 1988.

5. Ungar, E. E. and Williams, B. F., <u>A Study to Guide the Development and Use of Waveguide Absorbers for Structural Damping</u>, BBN Laboratories. Inc., Report 6463 Mar. 1987.

6. United McGill Corporation, 1501 Kalamazoo Dr., P.O.Box 909, Griffin, GA 30224, material part no. DM.

7. <u>3562A-Dynamic Signal Analyzer Operating Manual</u>, Hewlett Packard, Oct. 1985.

8. <u>Impulse Hammer Instrumentation for Structural Behavior Testing Model K291B Operating Instructions</u>, PCB Piezotronics, Inc., Nov. 1983.

INITIAL DISTRIBUTION LIST

No. Copies

1. Defense Technical Information Center
   Cameron Station
   Alexandria, VA 22304-6145   2

2. Library, Code 0142
   Naval Postgraduate School
   Monterey, CA 93943-5000   2

3. Dean of Science and Engineering, Code 06
   Naval Postgraduate School
   Monterey, CA 93943-5000   2

4. Research Administration Office, Code 012
   Naval Postgraduate School
   Monterey, CA 93943-5000   1

5. Department Chairman, Code 69
   Naval Postgraduate School
   Monterey, CA 93943-5000   1

6. Professor Young S. Shin, Code 69Sg
   Naval Postgraduate School
   Monterey, CA 93943-5000   4

7. Professor Kilsoo S. Kim, Code 69Ki
   Naval Postgraduate School
   Monterey, CA 93943-5000   1

8. Dr. Arthur Kilcullen, Code 1962
   David W. Taylor Naval Ship R&D Center
   Bethesda, MD 20084   1

9. Mr. Maurice Sevik, Code 19
   David W. Taylor Naval Ship R&D Center
   Bethesda, MD 20084   1

10. Mr. Gordon Eversteine, Code 1844
    David W. Taylor Naval Ship R&D Center
    Bethesda, MD 20084   1

11. Dr. Lawrence Maga, Code 196
    David W. Taylor Naval Ship R&D Center
    Bethesda, MD 20084   2

12. Dr. B. Whang, Code 1750.2   1
    David W. Taylor Naval Ship R&D Center
    Bethesda, MD 20084

13. Dr. Peter Doubleday   1
    Underwater Sound Research Detachment
    Naval Research Laboratory
    P.O. Box 8337
    Orlando, FL 32856

14. Dr. Alfred Tucker   1
    Office of Naval Research
    800 North Quincy St.
    Arlington, VA 22217

15. Mr. P. Majumdar, Code 55N   1
    Naval Sea Systems Command Headquarters
    Washington, DC 20362

16. Mr. Jerry Snyder, Code 55Y13   1
    Naval Sea Systems Command Headquarters
    Washington, DC 20362

17. Dr. N. T. Tsai   1
    Defense Nuclear Agency
    SPSS
    Washington, DC 20305-1000

18. Dr. Parviz Mahmoodi   1
    Building 201-BS-08
    3M Center
    St. Paul, MN 55144

19. LT Stephen J. Watson   1
    7 Snowfields Rd.
    Mattapoisett, MA 02739